AXIAL-FIELD PERMANENT MAGNET MOTORS

FOR ELECTRIC VEHICLES

Final Report

by

Dr. Peter Campbell,
Principal Investigator

for the period January 15, 1979 through September 30, 1981.

University of Southern California
Department of Electrical Engineering
Los Angeles, California 90007

Grant No. NSG-3243,

NASA-Lewis Research Center

SUMMARY

Axial-field permanent magnet motors have been shown to be particularly suitable for electric vehicle drives, as evidenced by the support for such advanced motors in the Department of Energy's Electric and Hybrid Vehicle Program. There were two most important factors in the analytical modeling of this type of machine that had not been extensively studied, and which were the subject of this research. These are:

(i) The modeling of anisotropic alnico-type permanent magnets. It is well-known that magnets with linear demagnetization characteristics can be simply modeled by an equivalent solenoid for the purposes of field computation. However, those with non-linear demagnetization curves are very much more difficult to model, since a non-uniform magnetization distribution exists throughout the magnet volume. This research was aimed at developing a realistic analytical model for such materials, which predominantly include the alnico types.

(ii) Modeling of the mechanical commutation in these motors. The high coercive force of permanent magnets allows large air-gaps to be tolerated, and this leads to the use of iron-less disc-type armatures and the axial-field

topology. The advantages are the elimination of eddy-current and hysteresis power losses, and the gaining of high motor power densities. However, the consequent field in the magnetic neutral regions and the low inductances of the armature coils leads to greater short-circuit currents during commutation. The predominant power loss in this machine is therefore associated with the mechanical commutation process, which is analysed and measured as part of this research.

The results of this research project have been written up in two major papers, the full texts of which are attached as the essence of this final report. These papers reflect the most important aspects of the work.

The first, entitled

"A MODEL OF ANISOTROPIC ALNICO MAGNETS FOR FIELD COMPUTATION,"

has been submitted to the I.E.E.E. for publication in the Transactions on Magnetics. It summarizes the text of the University of Southern California Ph.D. Thesis by Saad A. Al-Murshid, which has the same title.

The second, entitled

"COMMUTATION OF THE PERMANENT MAGNET AXIAL-FIELD D.C. MACHINE,"

has been submitted to the I.E.E. for publication in the proceedings part B. It summarizes the text of the University

of Southern California Ph.D. Thesis by Abdulhamid T. El-Kamodi, which has the same title.

A MODEL OF ANISOTROPIC ALNICO MAGNETS FOR FIELD COMPUTATION

Peter Campbell and Saad A. Al-Murshid

ABSTRACT

The modelling of an anisotropic alnico magnet for the purpose of field computation involves assigning a value for the material's permeability in the transverse direction. This is generally based upon the preferred direction properties, being all that are easily available. By analyzing the rotation of intrinsic magnetization due to the self-demagnetizing field, it is shown that the common assumptions relating the transverse to the preferred direction are not accurate. Transverse magnetization characteristics are needed, and these are given for Alnico 5, 5-7, and 8 magnets, yielding appropriate permeability values.

This work was supported by grant #NSG-3243 from the NASA-Lewis Research Center.

The authors were with the University of Southern California. Dr. Campbell is now with Patscenter International Inc., 707 Alexander Road, Princeton, NJ 08540, and Dr. Al-Murshid is with the Faculty of Engineering and Petroleum, Kuwait University, Kuwait City, Kuwait.

INTRODUCTION

In the calculation of magnetic fields in permanent magnet devices, modelling of the permanent magnet material itself usually relies upon data acquired from the major demagnetization curve. Most of the magnets used in electromechanical devices, such as rotating electrical machines, are anisotropic, and a curve measured in the preferred direction does not represent magnetic properties in any other direction. Unless the permanent magnet is subjected to a uniform self-demagnetizing field, some information on transverse magnetic properties will be required to find the complete field distribution. Of course, practical magnets do not approximate to the ellipsoidal shape required for a uniform internal field, and the boundary conditions, in addition to the magnet's anisotropy, will determine the extent of this field's non-uniformity.

This paper will briefly review the approximations that are commonly made to account for the transverse properties of a permanent magnet, leading to a comparison with actual characteristics measured on some popular materials. By considering the analytical derivation of anisotropy, a simple technique is suggested by which the directional magnetic properties may be more accurately represented in a field computation.

MAGNET FIELD EQUATIONS

The demagnetization curve for a permanent magnet relates the components of $\underline{B}$ and $\underline{H}$ for the preferred direction, and these vectors are also related to the material's intrinsic magnetization $\underline{M}$ via:

$$\underline{B} = \mu_0 (\underline{H} + \underline{M}) \quad . \tag{1}$$

It is convenient to express the dependence of $\underline{M}$ upon $\underline{H}$ as

$$\underline{M} = \underline{\chi}\,\underline{H} + \underline{M}_0 \quad , \tag{2}$$

and so

$$\underline{B} = \mu_0 \underline{\mu}' \underline{H} + \mu_0 \underline{M}_0 \quad , \tag{3}$$

where $\underline{\mu}' = (1+\underline{\chi})$ is an apparent relative permeability.

For an anisotropic material, $\underline{\chi}$ and $\underline{\mu}'$ are tensors, and may also be field dependent. However, the field quantities may be resolved into components in the preferred (p) and transverse (t) directions, so that

$$\underline{\chi} = \begin{bmatrix} \chi_p & 0 \\ 0 & \chi_t \end{bmatrix} \tag{4}$$

and

$$\underline{\mu}' = \begin{bmatrix} \mu'_p & 0 \\ 0 & \mu'_t \end{bmatrix} \quad . \tag{5}$$

This permeability tensor has been used to solve the field in regions containing soft-magnetic laminations [1], which are anisotropic but do not possess $\underline{M}_0$.

In permanent magnets, $\underline{M}_0$ must be assumed to act only in the preferred direction, to allow B_t and H_t to fulfill transverse symmetry conditions in the material. Hence,

$$\underline{M}_0 = \begin{bmatrix} M_{op} \\ 0 \end{bmatrix} \quad . \tag{6}$$

However, this does not mean that the intrinsic magnetization is fixed in the anisotropic direction, rather that any rotation of $\underline{M}_0$ will be accounted for by χ_p and χ_t.

In an isolated circular magnet (Fig. 1), the self-demagnetizing

$\underline{H}$ will only lie in the p-direction along the axis; elsewhere, there will also be a t-component of $\underline{H}$, leading to a rotation of $\underline{M}_0$ that is governed by the material's anisotropy. The equations of the magnetization curves for these mutually perpendicular directions are deduced from (2):

$$M_p = \chi_p H_p + M_{op} \tag{7}$$

$$M_t = \chi_t H_t \tag{8}$$

The major curve (7) is a commonly available design characteristic, and is measured with a uniform field, H_p, throughout the material. In contrast, little work has been done in the past to measure transverse properties.

It has been assumed [2] that the permeability functions μ'_p and μ'_t are the same, and even [3] that μ'_t is a constant, taking the value of μ'_p at remanence. The permeabilities to be used will actually depend upon the operating conditions of the magnet. If these are static, the major curves are appropriate, and if the material was initially saturated in the p-direction, operation will be on the demangetization curve for the p-direction and on the initial curve for the t-direction; these conditions also satisfy the symmetry requirements setting $M_{ot} = 0$. These magnetization curves have been measured for Alnico 5-7 (Fig. 2) and Alnico 8 (Fig. 3). Dynamic operation involves recoil, in the 2nd and 1st quadrants for p- and t-directions respectively, and a number of measured recoil loops are shown in Figs. 4 and 5 for the same materials. A constant value for relative recoil permeability may be assumed throughout any quadrant, provided that only small transverse fields exist, and Table I gives a comparison of the values. It is apparent from the measured characteristics that, dependent upon the material type, μ'_p and μ'_t may be quite dissimilar.

Table I: Relative recoil permeabilities measured from Figs. 4 and 5.

	p-direction, 2nd Quadrant	t-direction, 1st Quadrant
Alnico 5-7	1.82	6.70
Alnico 8	1.83	2.89

This use of the major magnetization curves implies that the p- and t-components are independent, which is in accord with (5). However, consider that in Fig. 1 there is a location at which only H_t exists. This will rotate $\underline{M}_0$ to give a component M_t as in (8), but (7) implies that M_p remains with value M_{op}. This is a contradiction, and clearly the application of H_t must reduce M_p by some amount. Therefore, (5) does not provide a complete model of a permanent magnet, and we should include at least the off-diagonal term μ'_{pt}, if not μ'_{tp} also. The more general permeability tensor is

$$\underline{\mu}' = \begin{bmatrix} \mu'_p & \mu'_{pt} \\ \mu'_{tp} & \mu'_t \end{bmatrix} , \qquad (9)$$

and we shall find values for all of these terms.

PERMANENT MAGNET ANISOTROPY

It may be shown that $\mu'_{pt} = \mu'_{tp} = 0$ for magnets operating on a linear demagnetization curve, such as the ceramic ferrites and rare earth-cobalts. This linearity is derived from a constant $M_p = M_{op}$, meaning that $\underline{M}_0$ is truly fixed in the p-direction. It is the rotation of $\underline{M}_0$ that yields a non-linear curve, in materials such as the alnicos. The

general case of an internal field $\underline{H}$ at angle θ_0 rotating the magnetization $\underline{M}_0$ by θ is shown in Fig. 6, and the energy associated with this field is:

$$E_f = \mu_0 H M_0 \cos(\theta_0 - \theta) \quad . \tag{10}$$

The torque that $\underline{H}$ applies to $\underline{M}_0$ is opposed by torques due to both shape and crystal anisotropy in alnicos. Considering that they have a cubic crystal lattice, the energies associated with these anisotropies are approximately given by [4]:

$$E_{sh} = K + K_{sh} \sin^2\theta \tag{11}$$

and

$$E_{cr} = K_0 + \tfrac{1}{4} K_1 \sin^2 2\theta \quad . \tag{12}$$

where K, K_{sh}, K_0, and K_1 are material anisotropy constants. The restoring torque on $\underline{M}_0$ is found from:

$$T = -\frac{\partial E_t}{\partial \theta} \quad ,$$

where E_t is the total of the energies in (10), (11), and (12). Hence,

$$T = -\mu_0 H M_0 \sin(\theta_0 - \theta) + K_{sh} \sin 2\theta + \tfrac{1}{2} K_1 \sin 4\theta \quad . \tag{13}$$

The usual technique for evaluating K_{sh} and K_1 is to rotate a thin disc of the material in a torque magnetometer, measuring T and θ_0. It is necessary to make $\theta_0 \simeq \theta$, and to eliminate the first term of (13), for which a uniform saturating field $\underline{H}$ is applied.

The typical operating conditions of a magnet in a device do not involve a saturating magnetic field, and so measurements of T vs. θ_0 cannot be interpreted. However, $\underline{M}_0$ and θ can be directly measured in

a vibrating coil magnetometer [5], in which a moderate $\underline{H}$ is applied parallel to the plane of the disc. Two sets of coils, in line with and at right angles to the field, provide signals from which $\underline{M}_0$ is deduced, as the sample is rotated through $-\theta_0$.

A disc of Alnico 5 has been tested in this way, and we shall consider results obtained in a moderate field of 30 kA/m, which is somewhat less than the value required for saturation. Figure 7 shows $|\underline{M}_0|$ vs. the angle of rotation of $\underline{H}$, θ_0, and Fig. 8 shows the angular difference between $\underline{H}$ and $\underline{M}_0$, $\theta_0 - \theta$ vs. θ_0. Shape anisotropy is predominant in Alnico 5, and $\underline{M}_0$ is much stronger in the p-direction than in the t-direction, with a preference for the axis of initial magnetization ($\theta_0 = 0$). As the sample (i.e., $\underline{H}$) is rotated through 180°, $\underline{M}_0$ stays closely aligned with $\underline{H}$ until the t-direction is approached, when $\underline{M}_0$ slips back almost to the preferred direction, and this is accompanied by the magnetization being nearly destroyed. However, as $\underline{H}$ approaches 180°, $\underline{M}_0$ reverses into alignment with $\underline{H}$ again, and the sample is partly remagnetized.

These results are interesting as an illustration of the rotation of $\underline{M}_0$, but because of the large values of $\theta_0 - \theta$ that occur, they cannot be used to find the anisotropy constants. Even in a saturating field, $\theta_0 - \theta$ is still not small enough to counter the large value of $\underline{H}$, to eliminate the first term of (13). Figures 9 and 10 show measurements at 211 kA/m, and now there is only a small variation in $\underline{M}_0$ with θ_0, the maximum $\theta_0 - \theta$ being 1.2° at $\theta_0 \approx 45°$. It will later be shown that K_{sh} and K_1 make the anisotropy energies small compared to the field energy here.

Unfortunately, the use of a magnetometer for permanent magnet materials does not yield the information needed to model their behavior, but we shall show that K_{sh} and K_1 may be derived from the major demagnetization curve. This is the same information from which μ'_t

was inaccurately deduced for field computation [2, 3], and we shall suggest a more accurate model based upon the same simple test. As seen from Fig. 1, typical values for θ_0 within a magnet are $150^\circ < \theta_0 < 210^\circ$. On the axis of symmetry, $\theta_0 = 180^\circ$, and we shall find from the intrinsic demagnetization curve that $H_{ci} = -53.7$ kA/m, the field required to reverse $\underline{M}_0$. However, we also saw in Fig. 8 that a similar sudden change in the direction of $\underline{M}_0$ occurs with a lower field, 30 kA/m, directed at $\theta_0 = 117^\circ$. In general, a steady, predictable rotation of $\underline{M}_0$ will only occur within limits of $|\underline{H}|$ and θ_0, and if $\theta_0 \neq 180^\circ$, the field at which a sudden change in θ occurs is less than H_{ci}.

ROTATION OF MAGNETIZATION

An analytical model for a permanent magnet should include the effect that $\underline{H}$ has upon $\underline{M}_0$. This may be found from (13), setting $T = 0$ to find the equilibrium position for $\underline{M}_0$. Thus,

$$\mu_0 H M_0 \sin(\theta_0 - \theta) = K_{sh} \sin 2\theta + \frac{1}{2} K_1 \sin 4\theta \quad , \tag{14}$$

which may be rearranged as

$$\frac{\mu_0 H M_0}{K_{sh}} \left[\frac{\sin(\theta_0 - \theta)}{\sin 2\theta} \right] - \frac{K_1}{K_{sh}} \cos 2\theta - 1 = 0 \tag{15}$$

If the magnitude and direction (θ_0) of $\underline{H}$ are known, and since $|M_0|$ is being considered a constant, this may be solved to give the rotation of $\underline{M}_0$ which is θ.

The critical field, H_c, at which the sudden change in θ occurs, is found by setting [4]:

$$\frac{\partial^2 E_t}{\partial \theta^2} = 0 \ .$$

Thus, from (13),

$$\mu_0 H_c M_0 \cos(\theta_0 - \theta) + 2K_{sh} \cos 2\theta + 2K_1 \cos 4\theta = 0$$

$$\therefore H_c = - \left[\frac{2K_{sh} \cos 2\theta + 2K_1 \cos 4\theta}{\mu_0 M_0 \cos(\theta_0 - \theta)} \right] \tag{16}$$

For the major demagnetization curve, $H_c = H_{ci}$, $\theta_0 = \pi$, and $\underline{M}_0$ is originally at $\theta = 0$, so

$$H_{ci} = \frac{2K_{sh} + 2K_1}{\mu_0 M_0} \ . \tag{17}$$

It is useful to think of intrinsic coercivities due to the shape and crystal anisotropies separately, being H_{cis} and H_{cic} respectively. H_{ci} becomes H_{cis} if $K_1 = 0$, and H_{cic} if $K_{sh} = 0$. Hence,

$$H_{ci} = H_{cis} + H_{cic} \ , \tag{18}$$

and (16) may be rewritten:

$$H_c = - \left[\frac{H_{cis} \cos 2\theta + H_{cic} \cos 4\theta}{\cos(\theta_0 - \theta)} \right] \ . \tag{19}$$

Thus, every angular rotation of $\underline{M}_0$ may be considered to be unstable if the critical field, H_c at θ_0, corresponding to that θ, is experienced.

It is more useful simply to know the value of H_c corresponding to any θ_0, for which θ must be eliminated. The second expression needed is (14), a general relationship between $\underline{H}$ and $\underline{M}_0$, which may similarly be rewritten as:

$$H = \frac{2H_{cis} \sin 2\theta + H_{cic} \sin 4\theta}{4 \sin (\theta_0 - \theta)} \quad . \tag{20}$$

The most familiar use of (19) is to draw the major demagnetization curve for $\theta_0 = \pi$, $\theta = 0$. This theoretical characteristic is simply a square loop, with $\underline{M}_0$ reversing abruptly between $\theta = 0$ and $\theta = \pi$ at $\pm H_{ci}$. The hysteresis loop for any other θ_0 is plotted by calculating H from (20) and the component of M at θ_0 from

$$M = M_0 \cos (\theta_0 - \theta) \quad . \tag{21}$$

The continuous range of H is determined by (19). Values for the constants are now needed.

From a large block of the same Alnico 5, small 10 mm cubes were cut at 10° increments (Fig. 11), and the intrinsic magnetization curves were measured (Fig. 12). Because of slight flaws in some of the cube samples, these curves do not exhibit an exactly steady progression. M_0 is taken as the saturation or spontaneous magnetization, and $\mu_0 M_0 = 1.334$ T. H_{ci} is measured from the major curve to be -53.7 kA/m. According to (11) and (12), only crystal anisotropy gives a stable energy condition in the t-direction, so the 90° demagnetization curve may be used to find $H_{cic} = -30.6$ kA/m, and hence $H_{cis} = -23.1$ kA/m.

With these values, analytical intrinsic magnetization curves may be plotted for different θ_0 as in Fig. 13. A study of these curves indicates any limitations in using (20) to model a real magnet. The most obvious discrepancy is the absence of remanence in the t-direction, which is because it was presumed that the spontaneous magnetization was in the p-direction. If the magnet were saturated with an H_t field, the crystal anisotropy would then yield such a remanence.

It has been mentioned that realistic conditions with a magnet will constrain $\underline{H}$ approximately to $150^\circ < \theta_0 < 210^\circ$. In fact, there is very good agreement between the measured and calculated remanence values in Figs. 12 and 13, from the 0° to the 60° curve, which encompasses $120^\circ < \theta_0 < 240^\circ$. Apparently the abrupt reversal of $\underline{M}_0$ does not occur in practice as predicted by (19), one reason being that the theory for shape anisotropy does not account for the interaction of neighboring magnetic elements in the non-magnetic material matrix.

This method of modelling a permanent magnet from the rotation of $\underline{M}_0$ does not require testing of the material in a magnetometer, and will therefore be relatively simple to implement. It was mentioned that K_1 and K_{sh} could not be evaluated in a torque magnetometer via (13), because the first term was not small. We now have these constants from Fig. 12, (17), and (18), which yield $K_1 = 20.4\ kJ/m^3$ and $K_{sh} = 15.4\ kJ/m^3$. These are small compared to $\mu_0 H M_0 = 281\ kJ/m^3$ at $H = 211\ kA/m$.

PERMANENT MAGNET MODEL

We have already developed an analytical model that requires information from only the p- and t-direction magnetization curves, and it will now be shown how just these need be used to evaluate the terms of (9).

Consider in Fig. 6 that $\underline{H}$ is applied at $\theta_0 = \pi/2$, for which (15) becomes:

$$\frac{\mu_0 H_t M_0}{K_{sh}} \frac{\cos\theta}{\sin 2\theta} - \frac{K_1}{K_{sh}} \cos 2\theta - 1 = 0 \qquad (22)$$

The t-component of $\underline{M}_0$ is found from (21) to be

$$M_t = M_0 \sin\theta \qquad (23)$$

Eliminating θ between these gives the transverse magnetization curve, M_t vs. H_t, from which χ_t is found. However, a simpler function will result if it is assumed that only a small rotation of $\underline{M}_0$ occurs, which is of course the case with anisotropic magnets in most practical applications. For small θ,

$$\frac{\mu_0 H_t M_0}{2 K_{sh} \theta} - \frac{K_1}{K_{sh}} - 1 = 0 \tag{24}$$

$$M_t = M_0 \theta \quad . \tag{25}$$

Eliminating θ,

$$M_t = \frac{\mu_0 M_0^2}{2(K_1 + K_{sh})} \quad H_t \tag{26}$$

$$\therefore \quad M_t = \left(\frac{M_0}{H_{ci}}\right) H_t \tag{27}$$

The rotation of $\underline{M}_0$ will be reflected as a reduction of M_p, such that

$$M_p^2 = M_0^2 - M_t^2$$

$$\therefore \quad M_p = M_0 \left(1 - \left(\frac{H_t}{H_{ci}}\right)^2\right)^{1/2}$$

Expanding this, remembering that $|\underline{M}_0| = M_{op}$, and approximating to the first term yields

$$M_p = M_{op} - \frac{1}{2} M_0 \left(\frac{H_t}{H_{ci}}\right)^2 \tag{28}$$

The permittivity functions may be written from (2) to include off-diagonal terms, as

$$M_t = \chi_t H_t + \chi_{tp} H_p \tag{29}$$

$$M_p = M_{op} + x_p H_p + x_{pt} H_t \tag{30}$$

Comparison between (27) and (29), and between (28) and (30) yields:

$$x_t = \frac{M_0}{H_{ci}} \tag{31}$$

$$x_{tp} = 0 \tag{32}$$

$$x_p = 0 \tag{33}$$

$$x_{pt} = -\left(\frac{M_0}{2H_{ci}^2}\right) H_t \tag{34}$$

For the t-direction, the theory assumes that the material was spontaneously magnetized in the p-direction, and so H_p alone will yield no M_t, which leads to (32). The initial curve is modelled by (31), which is the tangent to the 90^o curve in Fig. 13. This line coincides with the point at which saturation is achieved on the major (0^o) characteristic. For the Alnico 5, the value of (31) is 19.8, whereas the corresponding measured initial slope from Fig. 12 is 7.3. The discrepancy is due to the measured value of H_{ci} = 53.7 kA/m used in (31), and Fig. 12 shows that saturation actually occurs at a much higher field than this. There are two possible ways to achieve an accurate model of x_t.

If possible, the transverse magnetization characteristic should be measured, yielding x_t directly, but this may be inconvenient since alnico magnets are difficult to grind, and their application most often does not require parallel, ground sides. Alternatively, there is a general rule in the magnetization industry [6] that the field required to saturate an alnico is three times its coercivity. Surprisingly, this works very well here, and the transverse curve is not needed. The coercivity is derived from the major curve in Fig. 12 as 50.1 kA/m, and taking H_{ci} in (31) as

3x50.1 kA/m yields $\chi_t = 7.1$, compared to the measured 7.3. Either of these methods are a considerable improvement over existing techniques [2, 3], and for comparison, the measured slope of the major intrinsic curve at remanence is only 0.9.

For the p-direction, the assumption of spontaneous magnetization sets $\chi_p = 0$, whereas one might prefer to model the actual characteristic here as a function of H_p. Rotation of $\underline{M}_0$ will cause the magnet to operate within the major hysteresis loop, as this process involves the loss of some magnet energy. Dependent upon the transverse field H_t, M_p will be reduced according to (34), but to take better account of the actual characteristics, this should be rewritten as

$$\chi_{pt} = -\left(\frac{\chi_t}{2M_0}\right) H_t \tag{35}$$

Using the values found for χ_t and M_0 for Alnico 5, a field of $H_t = 30$ kA/m will cause only a 0.3% reduction in M_p. This is extremely small, and leads to the conclusion that although χ_{pt} is not actually zero, it may be assumed to be so.

The apparent relative permeabilities equivalent to these χ-functions are written by combining (29) and (30) with (1). The analytical form of (9) then becomes

$$\underline{\mu}' = \begin{bmatrix} 1 & -\dfrac{\chi_t H_t}{2M_0} \\ 0 & 1+\chi_t \end{bmatrix} . \tag{36}$$

However, in the light of the experiments described, it is preferable to use the measured p- and t-characteristics directly, in which case (9) reduces to its approximate form, (5).

Different investigators will have their own preferred methods for modelling the major demagnetization curve, with μ'_p as a function of H_p if necessary. Generally, though, information on transverse properties is not available, and we conclude with some further data obtained by grinding cubes of Alnico 5-7 and Alnico 8. Their magnetization curves were shown in Figs. 2 and 3 respectively. We have stated that symmetry requirements dictate the initial t-characteristic be used for static field applications, and this is approximately linear in small fields. The constant values of μ'_t that should be used in (5) are given in Table II.

Table II: Relative Initial Permeabilities Measured in the Transverse Direction.

Material	μ'_t
Alnico 5	8.3
Alnico 5-7	9.25
Alnico 8	1.9

CONCLUSIONS

Whereas it is common practice to set off-diagonal terms in the permeability tensor to zero, experimental data and analysis have been presented that justify this assumption. Moreover, important information on the transverse characteristics of the three most common permanent magnets will help to improve field computation. The values of μ'_t for Alnico 5 and 5-7 are particularly high compared to μ'_p, as was the case for recoil permeability, and this would tend to enhance transverse flux

in a magnet that directly experiences armature reaction in an electrical machine. If an exact model of a permanent magnet is required, then the rotation of $\underline{M}_0$ is found using (15) or (20).

REFERENCES

[1] A. Wexler, "Finite-Element Analysis of Inhomogeneous Anisotropic Reluctance Machine Rotor," IEEE Trans., PAS-92, 145-149, 1973.

[2] K. J. Binns and M. A. Jabbar, "Computation of the magnetic field of permanent magnets in iron cores," Proc. IEE, 122, 1377-1381, 1975.

[3] J. Slomczynska, "Non-linear analysis of the magnetic flux distribution in the magnetized magnet stabilized in air," IEEE Trans., MAG-10, 1109-1113, 1974.

[4] H. Zijlstra, "Experimental Methods in Magnetism," North-Holland, pt. 2, 168-208, 1967.

[5] G. C. Grimwood, A. M. Campbell, and J. E. Evetts, "Rotational Hysteresis in Polycrystalline Alloys," IEEE Trans., MAG-14, 359-361, 1978.

[6] F. Knight, "Magnetizing of Permanent Magnets," Permanent Magnet Association Tech. Bull., 7, 1966.

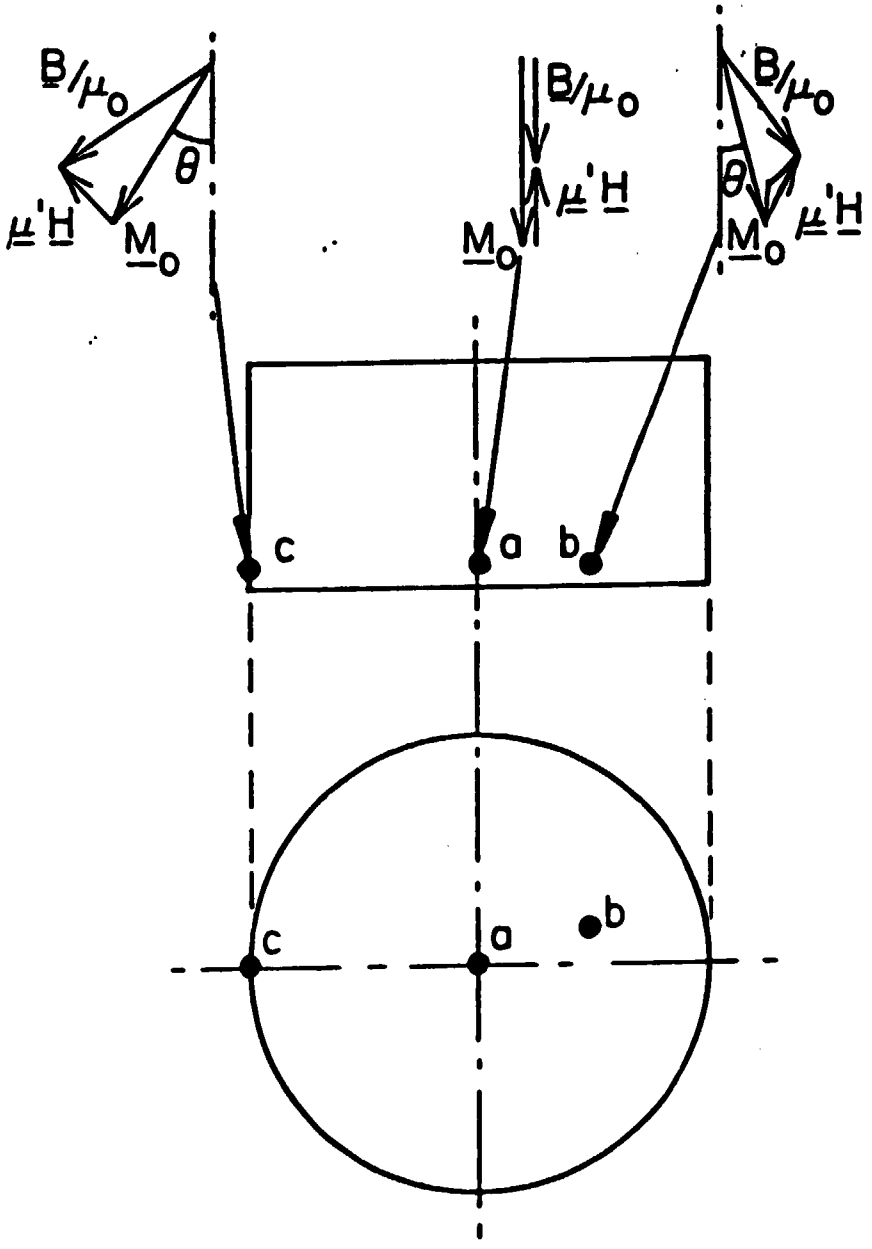

Fig. 1: Field within an isolated circular magnet.

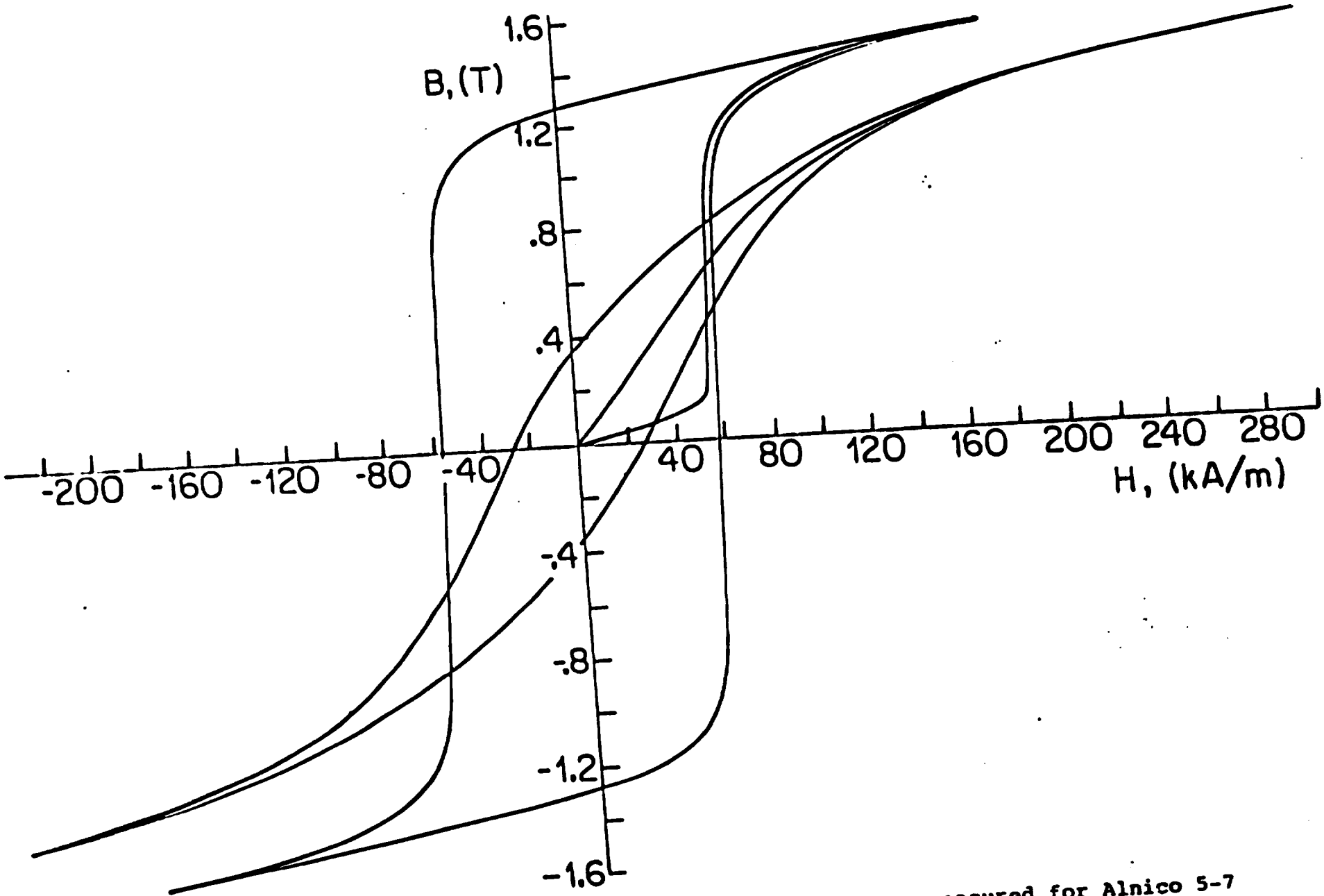

Fig. 2: Major magnetization curves measured for Alnico 5-7 in the preferred and transverse directions.

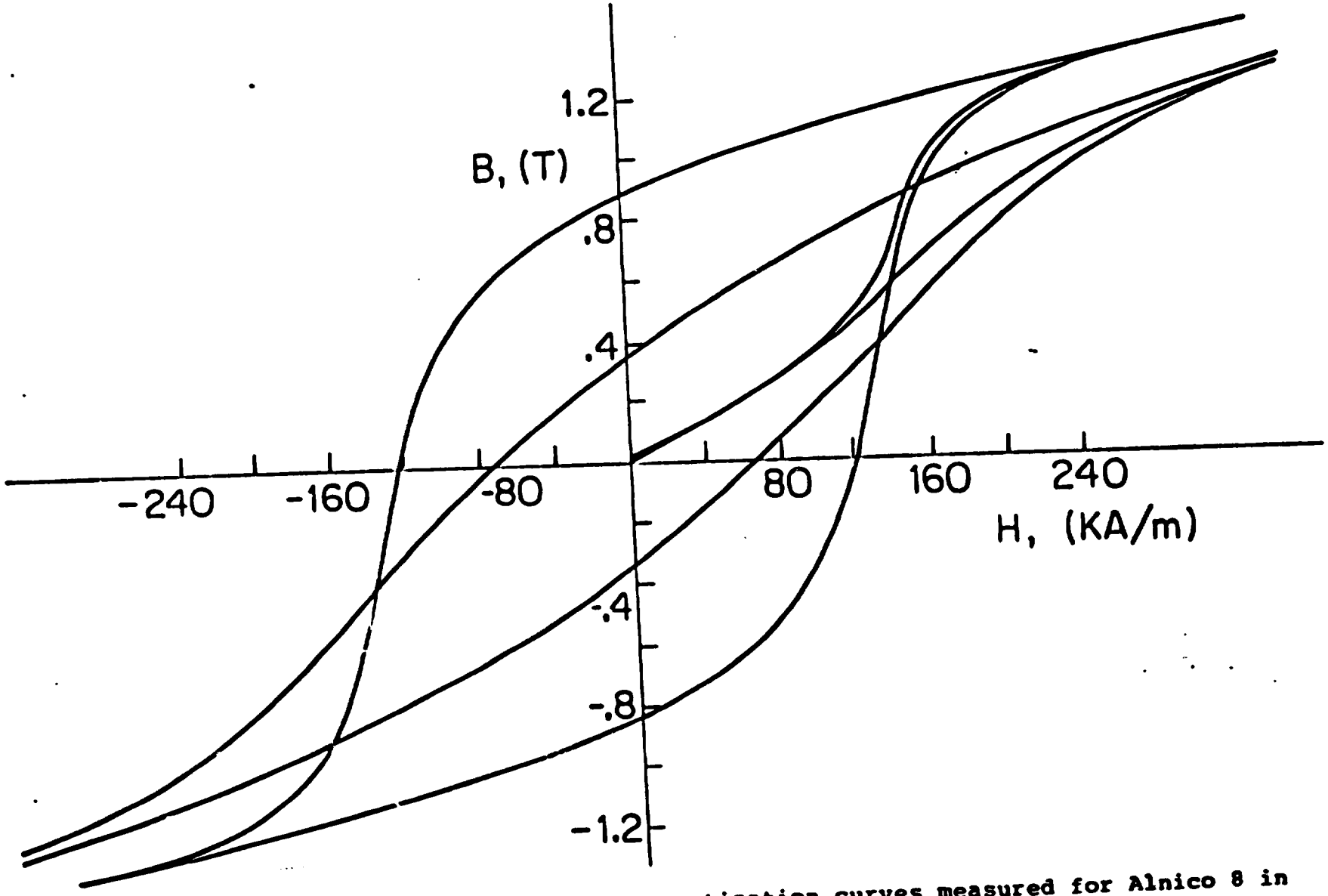

Fig. 3: Major magnetization curves measured for Alnico 8 in the preferred and transverse directions.

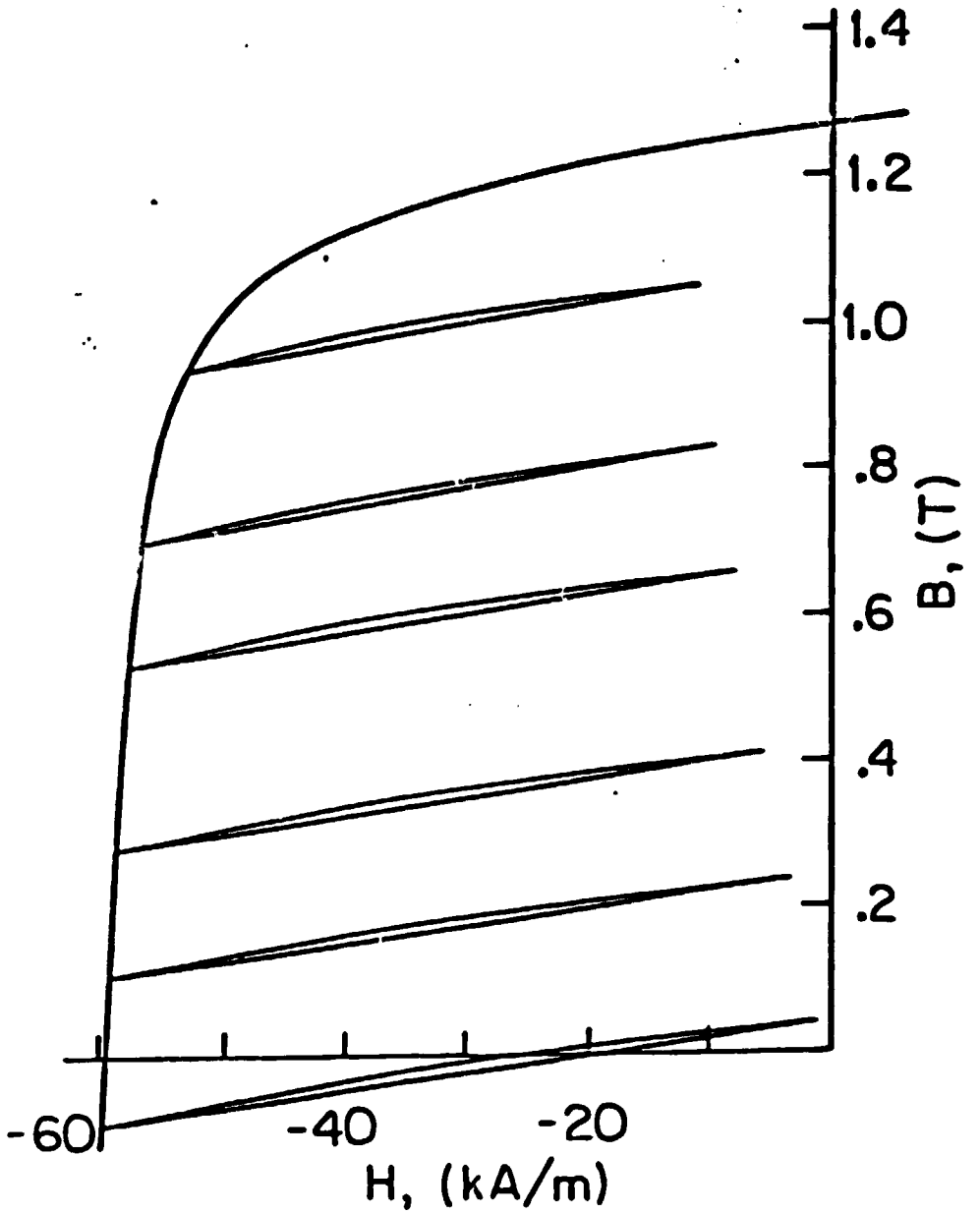

Fig. 4: Recoil loops measured for Alnico 5-7:
(a) preferred direction, in the second quadrant,

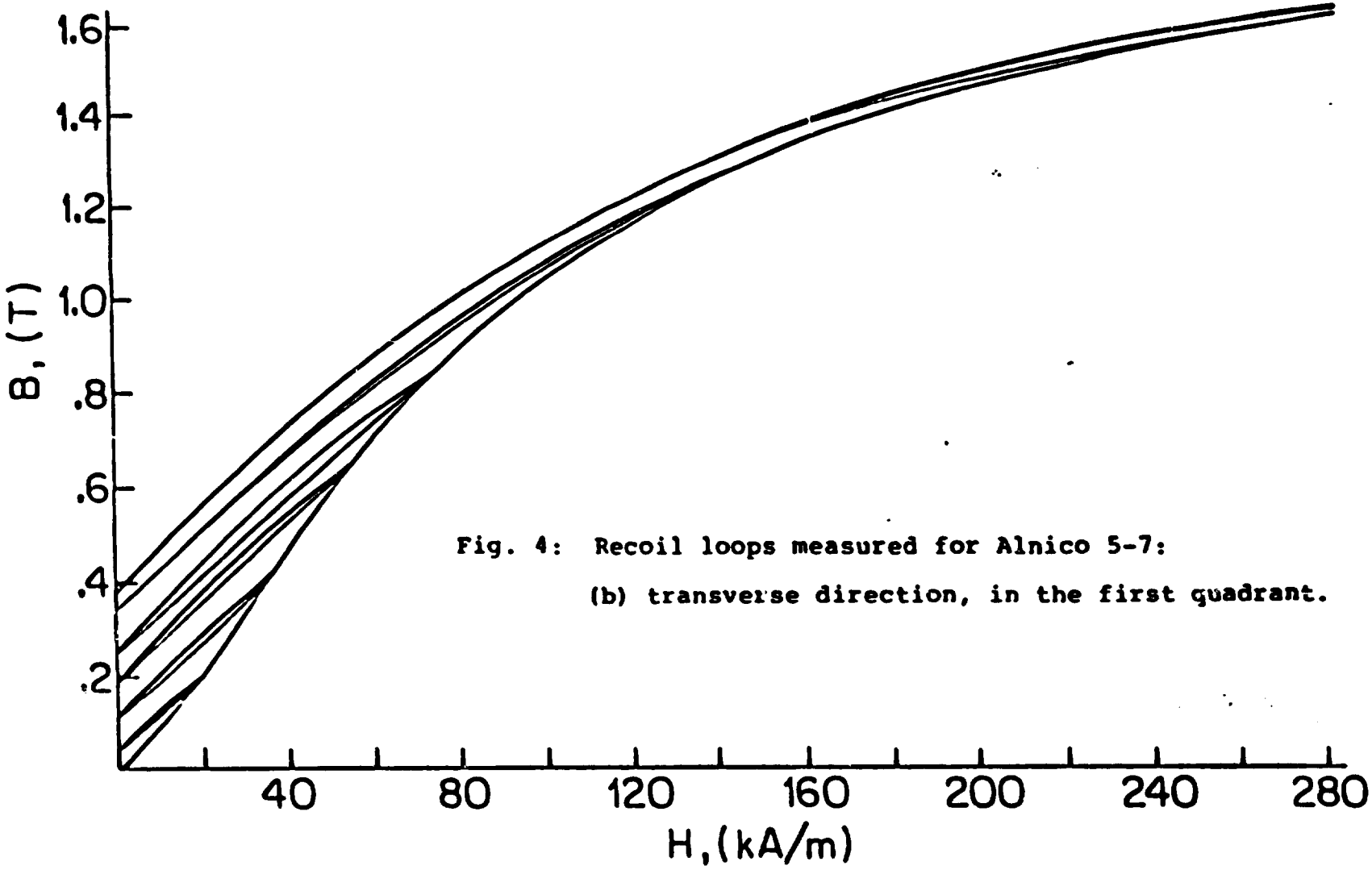

Fig. 4: Recoil loops measured for Alnico 5-7:
(b) transverse direction, in the first quadrant.

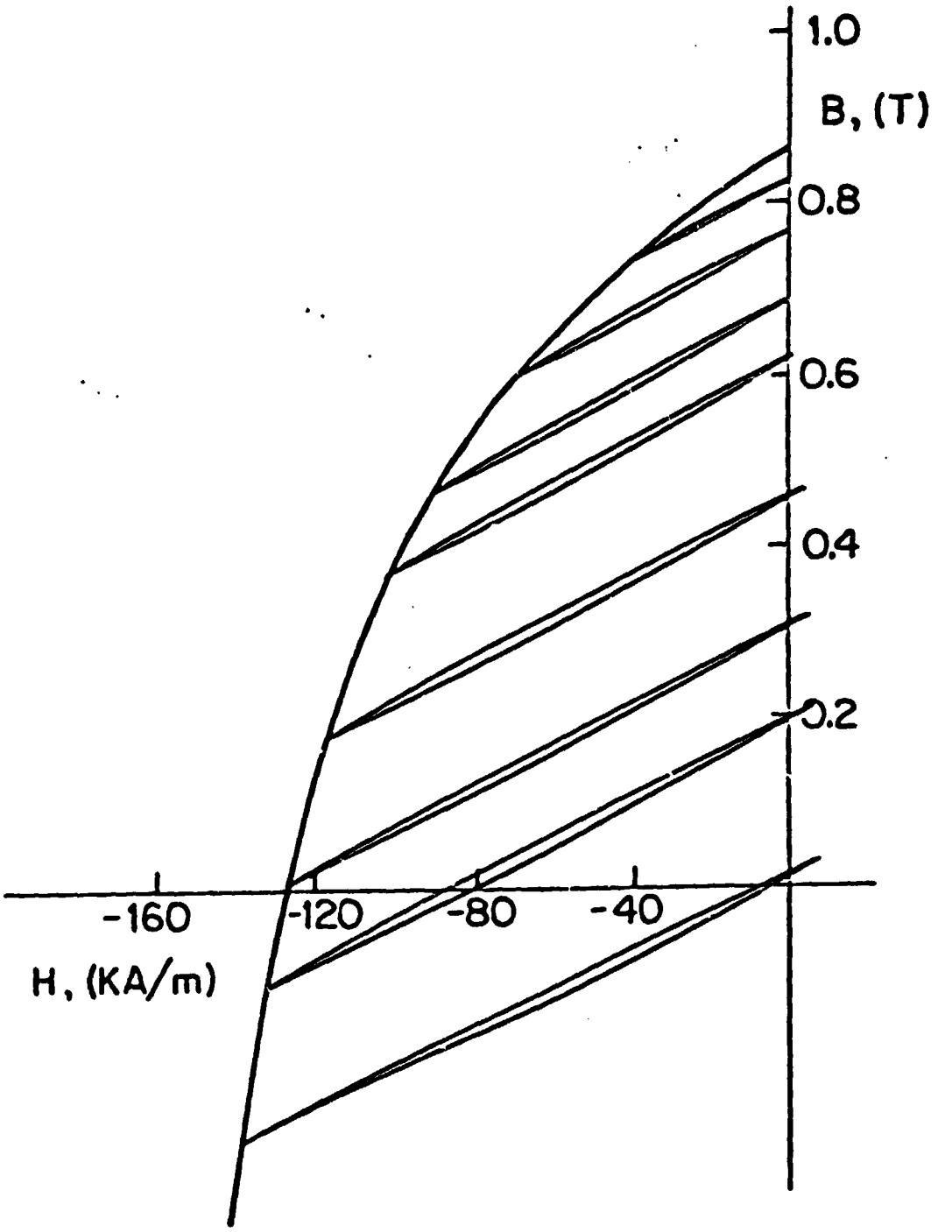

Fig. 5: Recoil loops measured for Alnico 8:
(a) preferred direction, in the second quadrant,

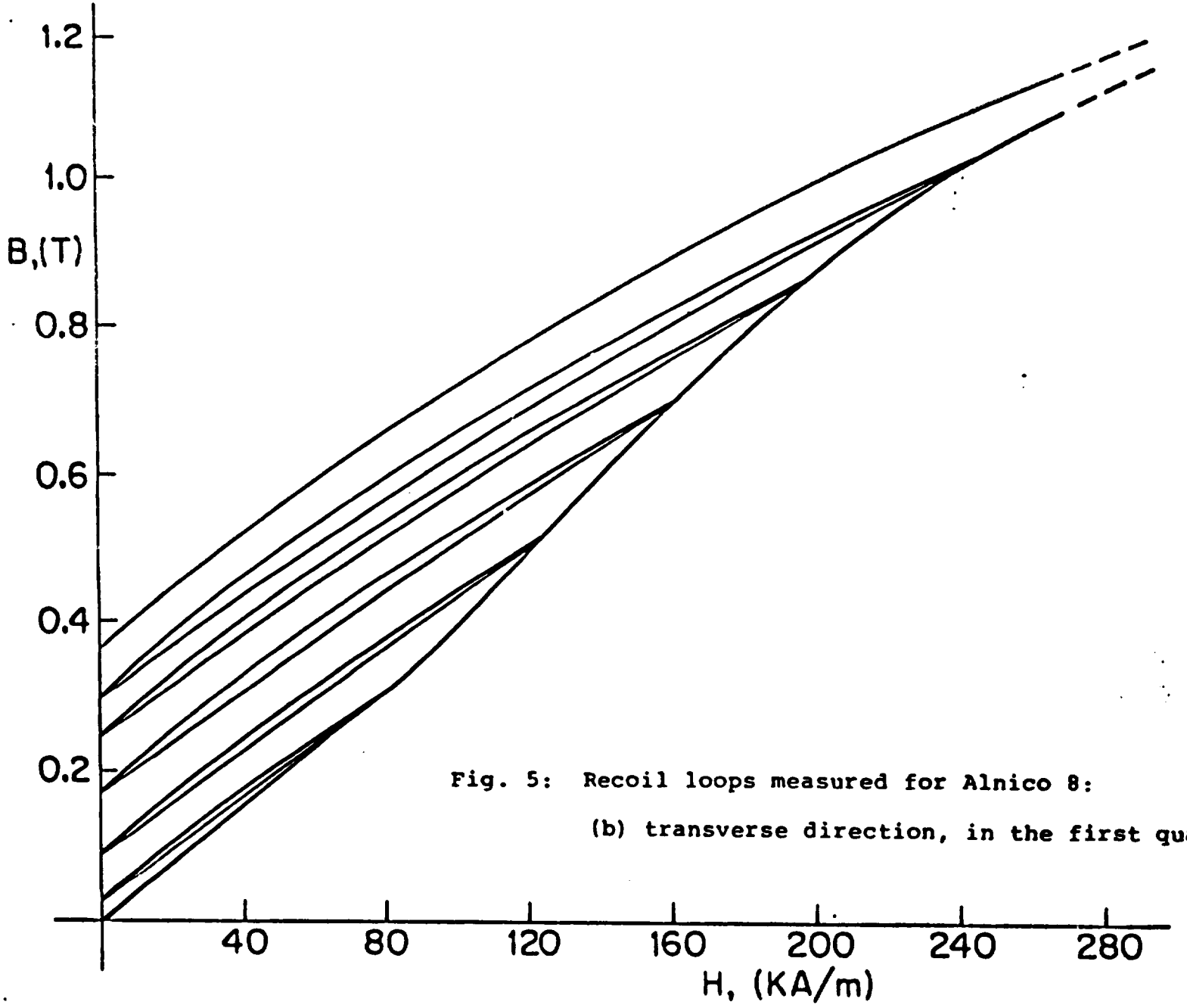

Fig. 5: Recoil loops measured for Alnico 8:

(b) transverse direction, in the first quadrant.

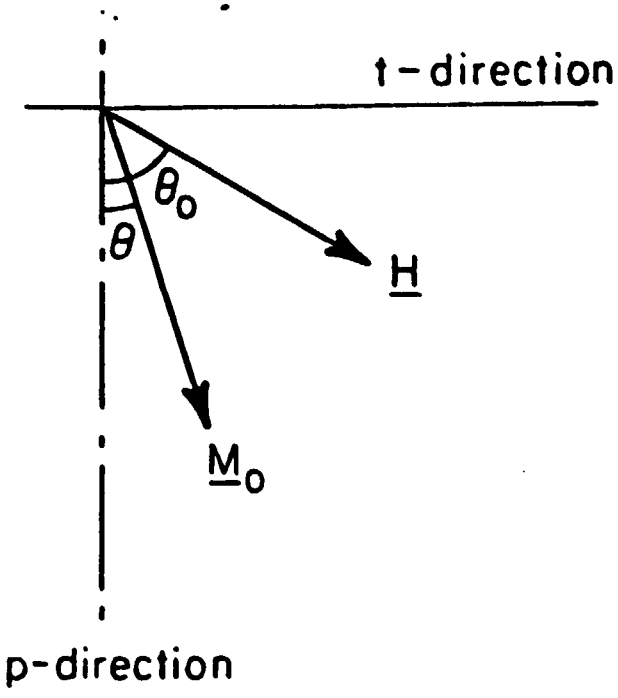

Fig. 6: Rotation of the magnetization $\underline{M}_0$ by an internal field $\underline{H}$.

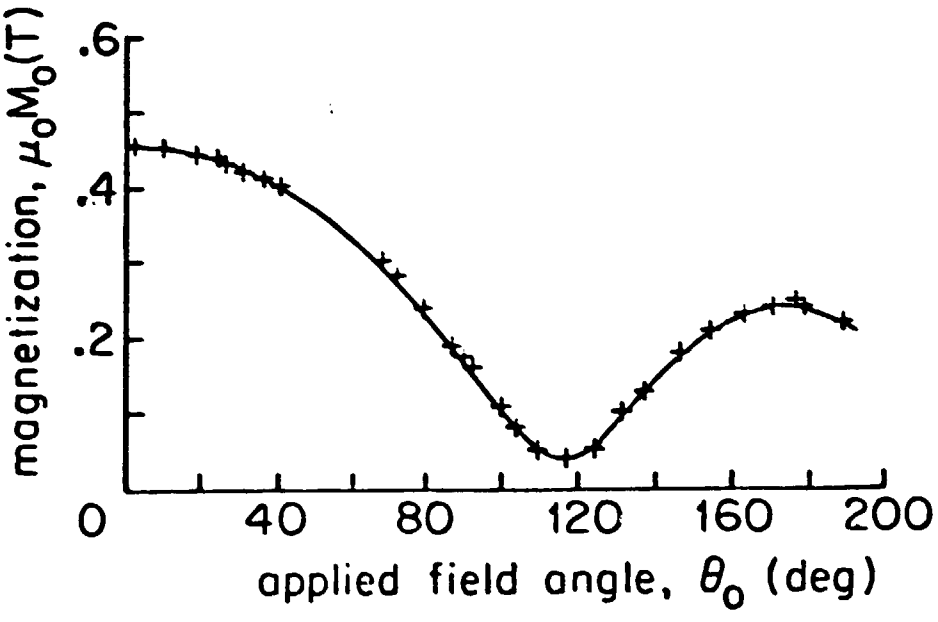

Fig. 7: Variation of $|\underline{M}_o|$ with rotation by θ_o of $\underline{H}$ = 30 KA/m, for Alnico 5.

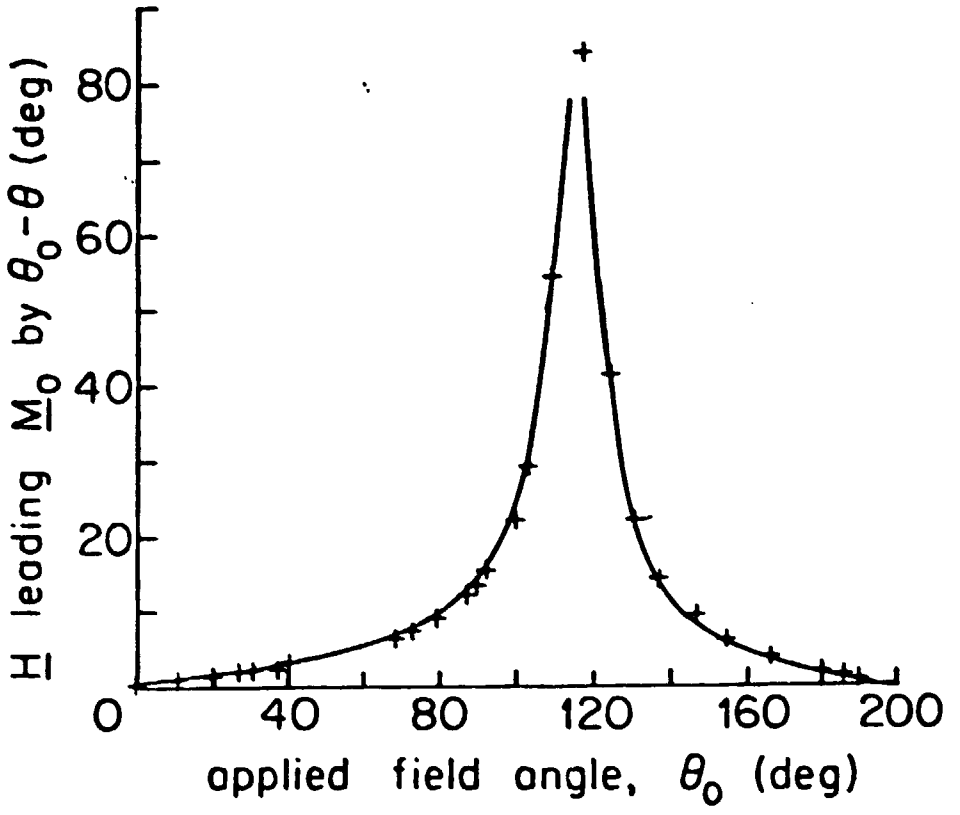

Fig. 8: Angle by which $\underline{H}$ leads $\underline{M}_o$, $\theta_o - \theta$, with rotation by θ_o of $\underline{H}$ = 30 KA/m, for Alnico 5.

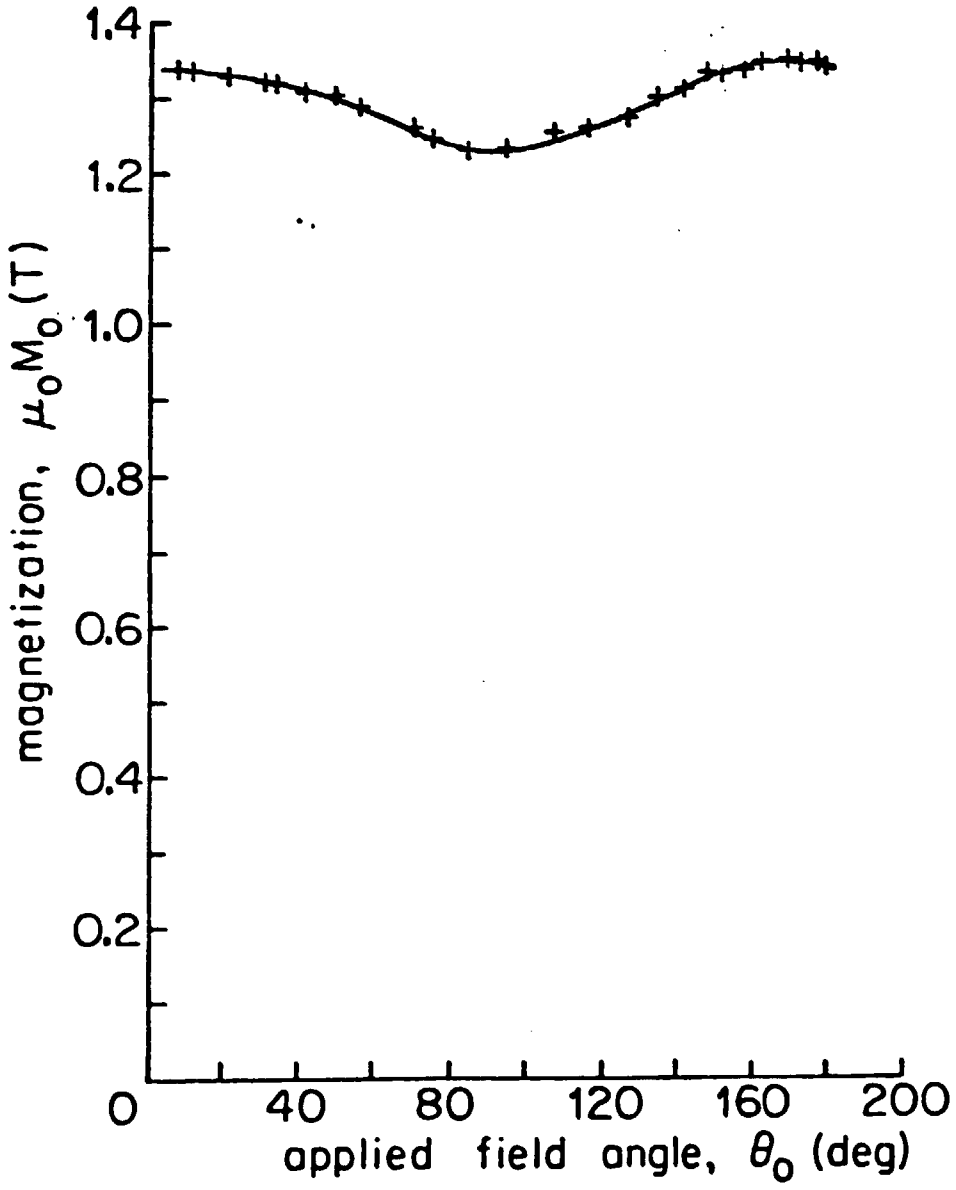

Fig. 9: Variation of $|\underline{M}_o|$ with rotation by θ_o of $\underline{H}$ = 211 KA/m, for Alnico 5.

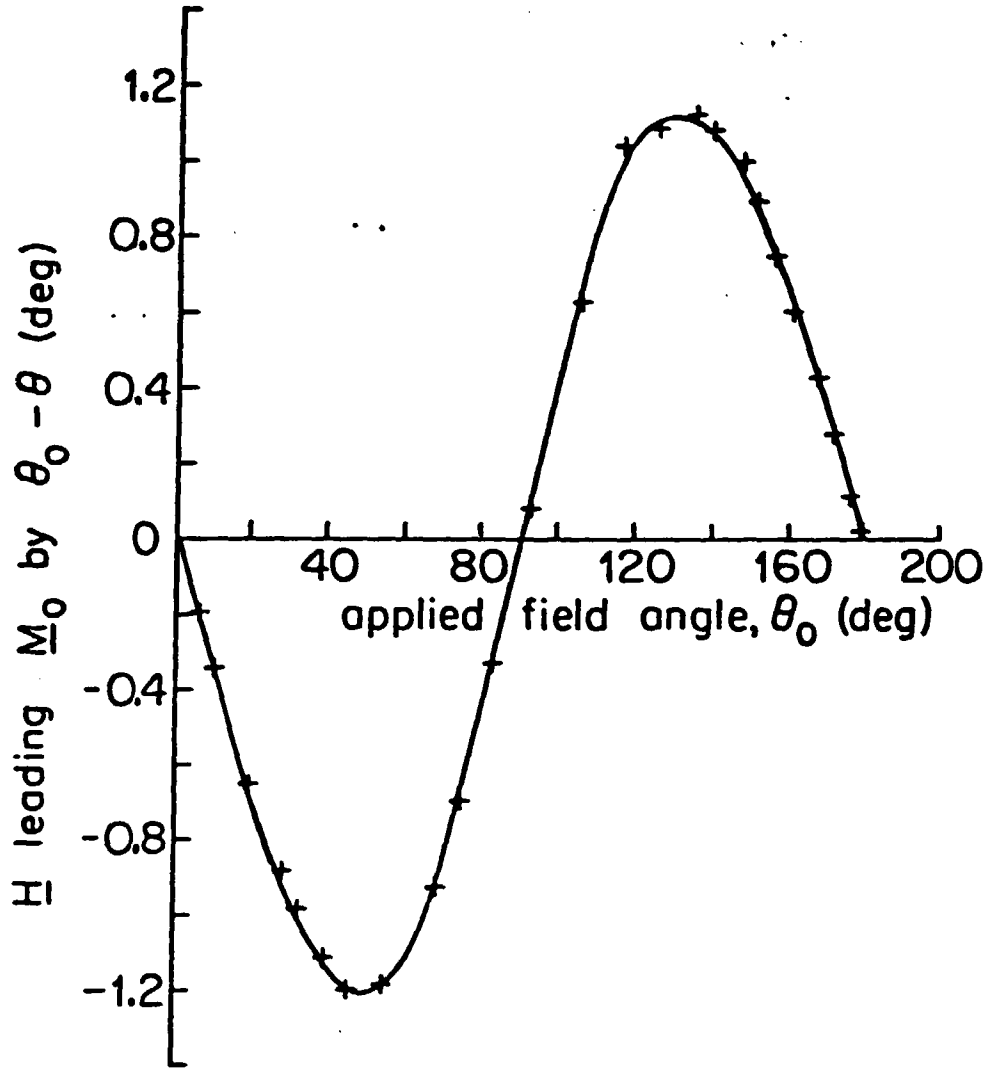

Fig.10: Angle by which $\underline{H}$ leads $\underline{M}_o$, $\theta_o - \theta$, with rotation by θ_o of $\underline{H}$ = 211 KA/m, for Alnico 5.

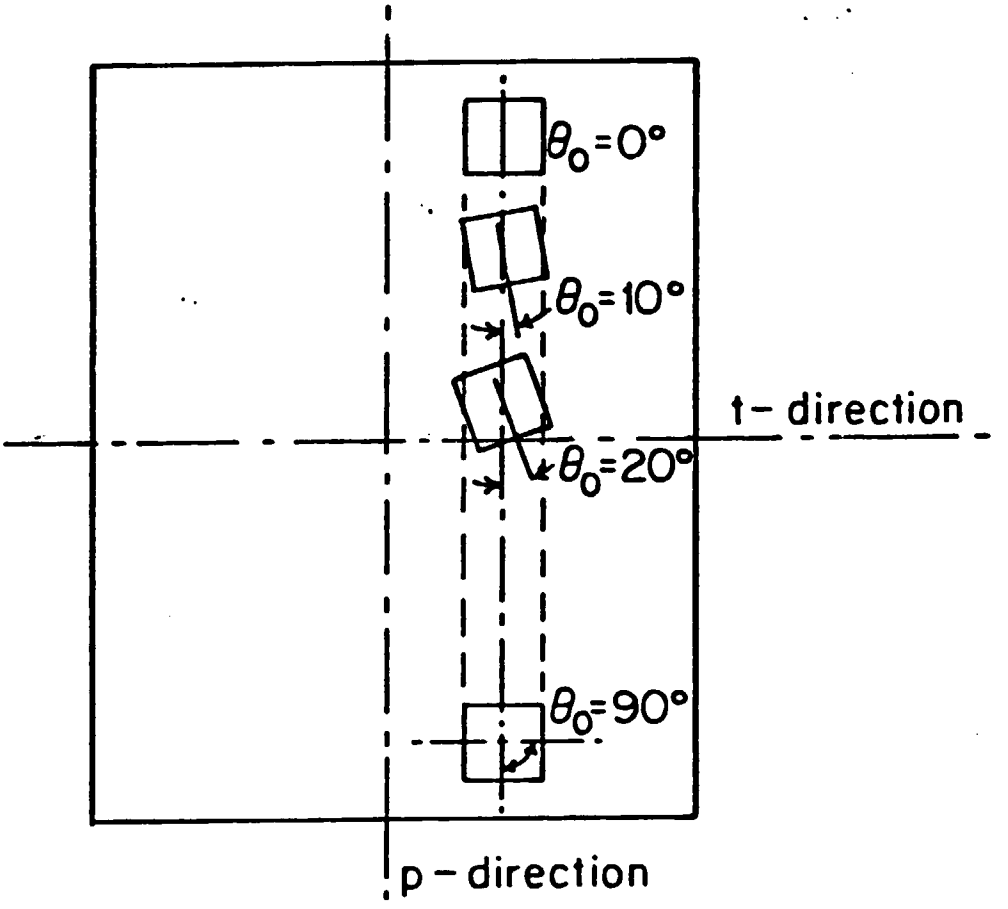

Fig.11: Cube samples cut at 10° increments from a block of alnico.

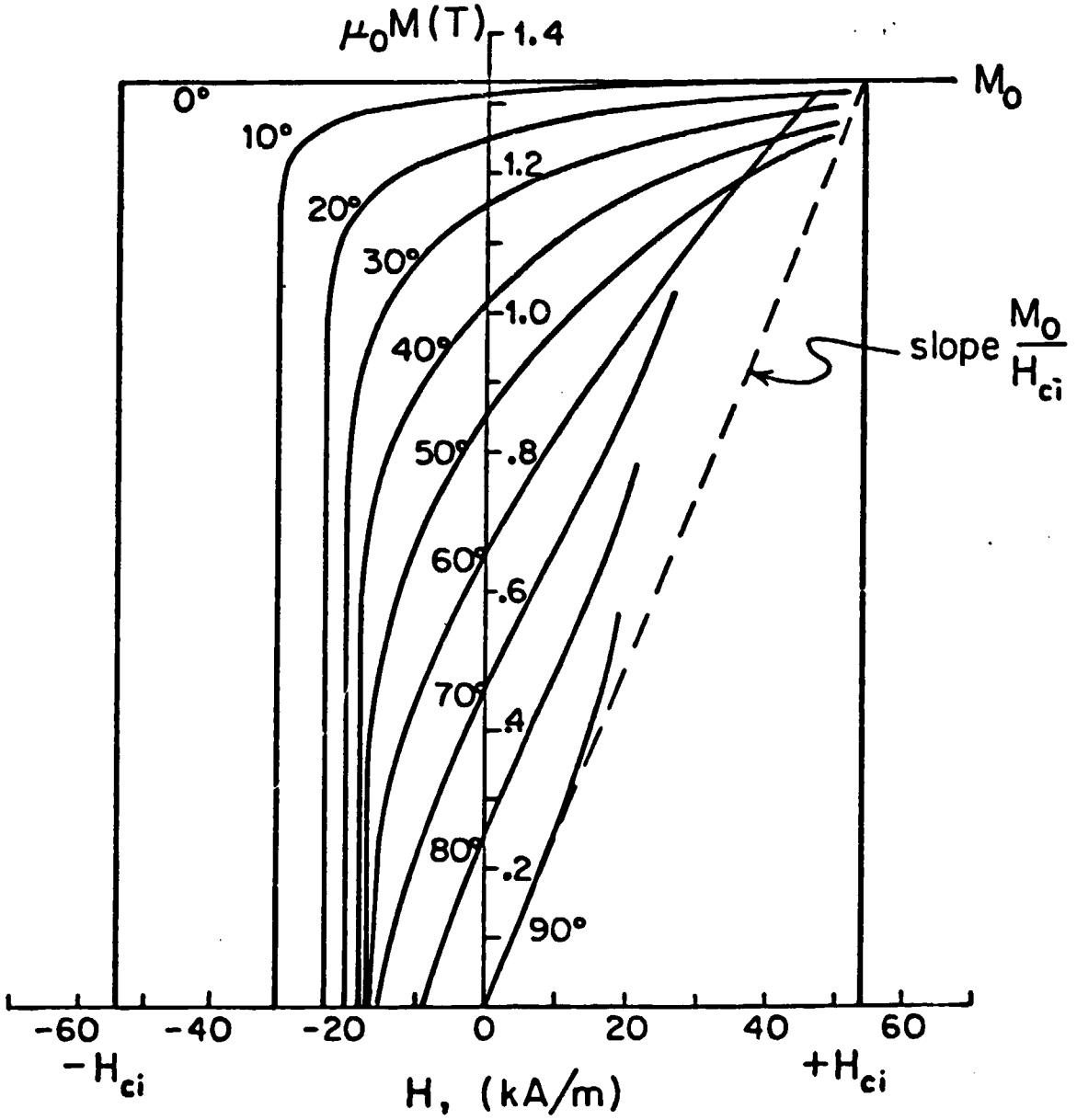

Fig.12: Intrinsic magnetization curves measured at various angles θ_o to the preferred direction in Alnico 5.

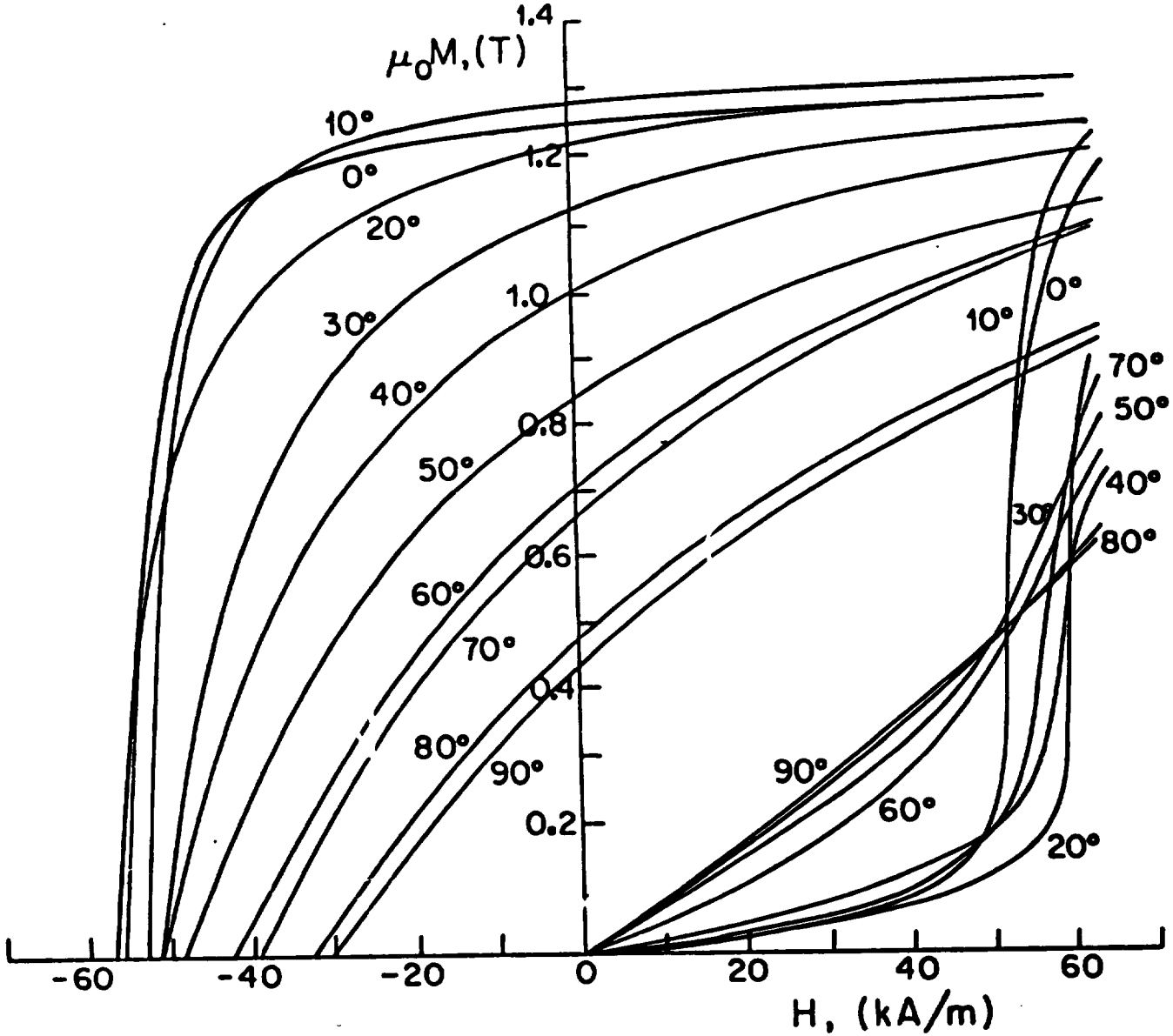

Fig. 13: Intrinsic magnetization curves calculated at various angles θ_o to the preferred direction in Alnico 5, using $\mu_o M_o$ = 1.334 T and H_{ci} = - 53.7 KA/m.

COMMUTATION OF THE PERMANENT MAGNET AXIAL-FIELD D.C. MACHINE

P. Campbell B.Sc., M.A., Ph.D., C.Eng., M.I.E.E.
and A.T. El-Kamodi, M.S., Ph.D.

ABSTRACT

The power losses in a permanent magnet d.c. disc-armature motor are analysed, and the predominant component is found to be due to short-circuit currents in coils undergoing commutation. Measurement of these currents shows their magnitudes to be greater than predicted from an equivalent circuit of the machine, and this suggests that the brush contacts may not be modeled by resistance alone. Inductances used in the equivalent circuit are very small, and their angular variations are found to depend upon the properties of the anisotropic alnico magnets; the transverse recoil permeability of Alnico 5-7 is about four times that in the preferred direction, giving some saliency.

Dr. Peter Campbell,
University of Southern California,
Department of Electrical Engineering, PHE 610,
Los Angeles, California 90007,
U.S.A.

List of Principal Symbols

e_1 = e.m.f. in one winding path.

e_c = e.m.f. in a single coil.

i = short-circuit current in a coil.

i_1 = mesh current in neighboring winding paths.

r_b = contact resistance between one brush and commutator.

r_{b1}, r_{b2} = contact resistance between one brush and one commutator segment.

r_c = coil resistance.

t_1, t_2 = time at onset and end of commutation.

$\underline{A}$ = vector magnetic potential.

$\underline{B}$ = flux density.

I = armature current.

$\underline{J}$ = winding current density.

L = coil self-inductance.

L_t = total self-inductance of two neighboring winding paths.

M = total mutual inductance between short-circuit coil and two neighboring paths.

$M2, M3$ = mutual inductance between short-circuit coil and first two neighboring coils.

P_{comm} = commutation power loss.

P_ℓ = constant term of power loss.

R = resistance added in series with coils.

R_a = total machine resistance.

γ = angular displacement between adjacent coils.

μ = relative permeability.

θ = angular position of short-circuit coil.

ω = armature angular velocity.

ϕ = total flux per pole.

1. Introduction

The permanent magnet d.c. disc-armature motor has a well-known topology,[1] a heteropolar axial-field magnet structure being adjacent to an ironless armature, the winding being encapsulated in epoxy resin. The characteristically long air-gap gives this machine a low armature inductance and a relatively high field about the magnetic neutrals. Both of these are expected to result in high power losses associated with the mechanical commutation process, and experiments on an early disc-armature motor have supported this view.[2] However, data acquired on that machine was limited because it was not possible to modify the armature for direct reading of currents.

The addition of resistors in series with one end of each coil and the commutator bars provides direct measurement of coil current via slip rings.[3] A variation on this technique is used with a specially constructed disc-armature motor, to verify computed short-circuit currents in a coil undergoing commutation, and thence to find the contribution that these make to the power losses in the machine. The experimental motor has eight poles, and a 72 coil lap-connected winding. After conventional steady-state load tests were performed, the armature was modified by the addition of the series resistors. Although only one resistor is connected to the slip rings for coil current measurement, a balancing resistor must usually be placed in all other coils.[3] However, the total addition to a winding path (9 coils) may adversely affect the performance of the machine.

The technique employed in this investigation involves the addition of

just one resistor to each parallel path, the value of 0.12Ω having little effect on performance and yet providing an adequate measurement signal. The armature of the experimental machine has an outer active diameter of 221mm (Fig. 1), and space is left between winding and commutator to accommodate the resistors and silver slip rings. Rather than having eight resistances, one added to every 9th coil, there being 9 coils/pole, there are nine resistances, one added to every 8th coil. The machine was constructed with brush arc and commutator segment arc equal, so that just one coil is commutated by each brush at any time. Therefore, at any time each parallel path has one added resistance, and one coil with a resistor is being commutated (Fig. 2). Balanced parallel winding paths are maintained while short-circuit coil current is recorded.

2. Equivalent circuit of the disc-armature motor.

An analytical technique is described for the evaluation of coil current and the associated power loss of commutation, for the axial-field permanent magnet d.c. machine. This will be verified by test data from the experimental motor.

The appropriate equivalent circuit for a coil undergoing commutation is shown in Fig. 3. This coil has resistance r_c, self-inductance L, and encounters an induced e.m.f. e_c. The particular coil under study will also have the added series resistance R, and the short-circuit current will flow through one resistive contact r_{b1} to the brush, returning through another contact r_{b2}. The circuit includes the neighboring armature paths, each of which

shares mutual inductance ½M with the commutating coil. Since this is a lap winding with an exact number if coils per pole, each neighboring path has approximately the same e.m.f. e_1, self-inductance ½L, and resistance $8r_c + R$ (9 coils/pole less one being commutated). No field winding appears in tne equivalent circuit, but if the permanent magnet material is an alnico type, there will be a salient-pole structure which will cause the inductances to be dependent upon the armature's angular position. Because of symmetry between the neighboring paths, each parameter in one will be equal to that in the other.

By suitable choice for the mesh current i_1 in Fig. 3, the terminal voltage V is eliminated and the e.m.f.s e_1 cancel. The two mesh equations in i and i_1 are

$$\left(R + r_c + r_{b1} + r_{b2} + \frac{dL}{dt}\right) i + L\frac{di}{dt} + M\frac{di_1}{dt} + \left(\frac{dM}{dt} - r_{b1} - r_{b2}\right) i_1 = e_c \qquad (1)$$

$$\left(\frac{dM}{dt} - r_{b1} - r_{b2}\right) i + M\frac{di}{dt} + L_t\frac{di_1}{dt} + \left(2R + 16r_c + 2r_{b1} + 2r_{b2}\right) i_1 = 0. \qquad (2)$$

These may be solved for the short-circuit current i, provided that all of the resistances and inductances are known.

2.1. Resistances.

The resistance of a winding path is simply measured by a static drop-test at rated current, from which r_c is deduced as 0.042Ω. Brush contact resistance, however, will vary both with angular velocity and angular position

of the armature. The study of brush contact phenomena is alone a most involved subject,[4] and a simplified representation was employed for modeling this machine. It was assumed that the contact resistance between a brush and a commutator segment is inversely proportional to the contact area, and that r_{b1} and r_{b2} (Fig. 3) vary with angular position ωt according to

$$r_{b1} = r_b \frac{\omega t_2 - \omega t_1}{\omega t - \omega t_1} ; \quad r_{b2} = r_b \frac{\omega t_2 - \omega t_1}{\omega t_2 - \omega t} , \qquad (3)$$

where $t_1 < t < t_2$. t_1 and t_2 give the times at the onset and end of commutation for the coil under study. The parallel combination of r_{b1} and r_{b2} is r_b, which is independent of t; this is the effective resistance seen through a brush, which may be deduced from load tests on the motor. This procedure is described in sec. 3, from which the variations in r_{b1} and r_{b2} are found with the aid of Eq. (3).

2.2 Coil e.m.f.

To obtain the greatest power output from the experimental machine with the given armature, the highest possible air-gap flux density should be obtained. This is achieved with high remanence Alnico 5-7 permanent magnets, assembled in two sets, one on either side of the armature. This arrangement is preferable to having a single magnet set to one side and a steel ring on the other, as described in Ref. 2, as it reduces the leakage flux.

Because the ironless motor of the disc-armature machine ensures that negligible armature reaction occurs, a slow measurement of flux linking on actual coil may be used to determine the e.m.f., e_c. The flux variation was found to be almost exactly sinusoidal, which is typical of this type of

motor with a large air-gap. The experimental machine has 8 poles, the peak flux linking a coil is $\Phi = 10.55$ mWb, and so the coil e.m.f. is given by:

$$e_c = 4\omega\Phi.\cos 4\omega t$$
$$= .042\omega.\cos 4\omega t. \qquad (4)$$

The armature angular velocity is ω (rad/sec), and commutation occurs about the magnetic neutrals, corresponding to $\omega t = \pi/8, 3\pi/8, 5\pi/8$, etc. The salient pole structure and the much smaller air-gap length of conventional small d.c. machines tend to supress the coil e.m.f. somewhat during commutation, which is in contrast to the rapid increase in e.m.f. about the neutrals indicated in Eq (4). Acting in conjunction with low inductance values, this is the cause of significant short-circuit power losses in the disc-armature motor.

2.3 Inductances, considering Permanent Magnet Properties.

Calculation of the self and mutual inductances of an armature coil involves evaluation of the field resulting from rated current in the coil. The permanent magnets are immediately adjacent to the armature; if these were rare earth-cobalt or ferrite magnets, they would appear to the coil as air-gap, but alnicos have non-linear demagnetization characteristics. The relative permeability, μ, is variable along the B-H curve of an alnico and the recoil permeability is also different from unity. The consequent salient-pole structure gives all the inductances their angular dependence.

Many alnico magnets are also anisotropic, as seen by the major B-H

loops of Alnico 5-7 in the preferred and transverse directions (Fig. 4). These curves were measured on the actual material used for the experimental machine, one magnet being ground to a cube for testing in a permeameter. The conventional method of modeling such magnets that are subjected to an external field, as by armature coil, is just to use the recoil permeability from the second quadrant of the major B-H loop. Some recoil loops for the Alnico 5-7 magnet are plotted in Fig. 5, for which a constant recoil permeability of 1.82, the mean value, may be taken as a good approximation.

However, it is well-known that field within a non-linear permanent magnet may not be constrained to the preferred direction,[5] and so transverse components must be considered. In this case, the first quadrant of the magnetization loop should be used with recoil coming from the virgin curve. This is to satisfy the necessary conditions of symmetry about some plane within the magnet where no transverse field exists. Figure 6 gives the measured recoil loops for the Alnico 5-7 magnet, and since only small transverse fields will generally occur, a constant value of 6.70 may be taken for the recoil permeability.

The recoil permeability used to model Alnico 5-7 is therefore almost four times greater in the transverse direction than in the preferred direction. Remembering that alnico permanent magnets are generally many times longer than the air-gap, and that the steel backing rings are well removed from the region, it is possible that the self-inductance of a coil may be greater with its axis over the magnetic neutral than with it over the magnet center-line. This is contrary to the situation in a conventional

salient pole machine.

Since the active conductors in the axial-field machine lie radially, an approximate field distribution in the air-gap region may be found from a numerical solution of Poisson's Equation in 2-dimensions, at a fixed radius. The appropriate form of this will take account of the directional dependence of the permeability μ in the magnets, so that the flux density $\underline{B}$ is calculated via vector potential $\underline{A}$ from the current density distribution $\underline{J}$, using

$$\nabla \times \underline{B} = \underline{A} \tag{5}$$

and

$$\nabla \times \frac{1}{\mu} \left[\nabla \times \underline{A} \right] = \mu_0 \underline{J}. \tag{6}$$

Figure 7 shows a typical field distribution calculated at the average active radius for rated current in a coil, whose axis is midway between the magnetic neutral and the magnet center-line. The effect of having the higher transverse permeability is to shunt magnets in the vicinities of the conductors. Here we are evaluating inductance; however, it is fortunate that armature reaction is small in this machine, because otherwise this effect would seriously complicate any attempt to calculate the resultant (permanent magnet plus armature reaction) field distribution.

Account was also taken of end-winding effects, but since these are well removed from any magnetic materials, their contribution to inductances was found to be small. The angular variations of inductances (Fig. 8), determined from calculated field distributions, do verify that the

principal inductances are greatest with the coil axis over the magnetic neutral regions. The self-inductance L for this 8 pole machine may be written as the series

$$L = L_0 + L_1 \cos 8\omega t + L_2 \cos 16\omega t + L_4 \cos 32\omega t, \qquad (7)$$

where $L_0 = 8.06\mu H$; $L_1 = 1.76\mu H$; $L_2 = -.46\mu H$; $L_4 = .16\mu H$.

Mutual inductance with a neighboring coil depends both upon $\theta = \omega t$, the position of the source coil, and the relative position between the pair of coils. There is a strong coupling of the sinusoidal variation with the immediate neighbor, M2, and also with the coil that is exactly one pole pitch away, M10.

Measurements of inductance were obtained by constructing an armature, identical to that in Fig. 1, but without a commutator and hence without interconnections between coils. Assembled in the stator of the experimental machine, with one coil excited at rated current, the actual variations of inductance with angular position were found directly (Fig. 9). These all have extremely low values, characteristic of the ironless rotor permanent magnet machine, and are generally less than the calculated figures. The discrepancy is due to having taken a two-dimensional field approximation, neglecting the effect of the magnet boundaries at the inner and outer active radii. A three-dimensional field computation should yield more accurate results.[6]

For the parameters to be used in Eqs. (1) and (2), it is assumed

that L, M2 and M3 (the first two neighbors), have purely sinusoidal variations with ωt, higher harmonics being ignored; mutual inductance with all other coils is taken as constant. From the results of Fig. 9,

$$L = L_0 + L_1 \cos 8\omega t \tag{8}$$

$$M2 = M2_0 + M2_1 \cos 8(\omega t + \tfrac{1}{2}\gamma) \tag{9}$$

$$M3 = M3_0 + M3_1 \cos 8(\omega t + \gamma) \tag{10}$$

where $L_0 = 7.785\mu H$; $L_1 = .225\mu H$;

$M2_0 = 3.64\mu H$; $M2_1 = .51\mu H$;

$M3_0 = 2.61\mu H$; $M3_1 = .24\mu H$.

If two adjacent coils are displaced by an angle γ, being 5^0 in this 72 coil winding, the peak mutual inductance between them will occur at $\frac{1}{2}\gamma$ from the position corresponding to the peak self-inductance (Eq. 9). Similarly, with M3 the variation is shifted by 2 x $\frac{1}{2}\gamma$ in Eq. (10).

The total self-inductance, L_t, of the sixteen coils in the two neighboring armature paths in Fig. 3 is deduced from Eq. (8) to be

$$L_t = 16L_0 + 2L_1 \sum_{n=1}^{8} \cos 8(\omega t + n\gamma) \tag{11}$$

Similarly, the total mutual inductance linking these paths to the short-circuited coil is found using Eqs. (9) and (10) to be

$$M = 2\sum_{N=2}^{9} MN_0 + 2M2_1 \cos 8(\omega t + \tfrac{1}{2}\gamma) + 2M3_1 \cos 8(\omega t + \gamma) \tag{12}$$

The first term is evaluated from Fig. 9 as 47.3μH.

An important conclusion of this analysis is that, when an electrical machine topology involves alnico-type permanent magnets adjacent to the armature, consideration must be given to the magnetic characteristics perpendicular to the preferred (anisotropic) direction. Calculation and measurement of inductances has demonstrated the importance of field traversing the magnet faces. In Sec. 4, the calculated short-circuit current during commutation is compared favorably with measured variations.

3. Determination of Motor Parameters and Performance.

It was stated in Sec. 2.2 that the brush contact resistance will vary with angular position according to Eq. (3), averaging to a value of r_b at each brush; it will also be dependent upon the motor's speed. It will therefore be necessary to perform a load test on the motor at a constant speed, to determine the resistance that is associated with that speed.

The experimental disc-armature motor is shown in Fig. 10, the armature of Fig. 1 being located between the two sets of Alnico 5-7 magnets. In addition to the added resistors (R) in the winding, there is a 0.2Ω resistance (mounted above the machine in Fig. 10) in series with each brush lead for measurement of the brush current. The windings on the permanent magnets are for the purpose of initial magnetization only.

Rated voltage and speed for this machine are 60V and approximately 2400 rev/min. A load test at this constant speed yields the relationship between the total power losses and the square of armature current (I^2) given in Fig. 11. Except at very low current, the losses may clearly be

represented by a constant term, P_ℓ = 192W, and a constant resistance, R_a = .309Ω. P_ℓ is conventionally treated as a mechanical loss torque, $T_\ell = P_\ell/\omega$, and R_a accounts for all the electrical losses at this speed. An expression for the power losses involving output torque, T, is:

$$VI - \omega T = I^2 R_a + P_\ell. \tag{13}$$

Considering the values for the individual resistances in this eight pole lap-wound machine, given here and in Sec. 2.1, the total resistance of R_a = .309Ω breaks down into the following components:

(i)	armature winding resistance, including additional R in each path:	.057Ω
(ii)	total brush contact resistance:	.152Ω
(iii)	external resistances	.100Ω
Total:		.309Ω

At each brush contact, we deduced a value for r_b = .304Ω, which is to be used in Eq. (3) to solve for the short-circuit current from Eqs. (1) and (2).

The complete performance characteristics on this motor at 60V are given in Fig. 12, and over the measured current range, speed is seen to vary between rated speed and 11% less than this. Extrapolation of the speed curve to a very high stall current is characteristic of permanent magnet d.c. motors. With such a small variation in speed over this current range, we would expect good correlation between the power losses here and those at 2400 rev/min in Fig. 11.

This is so, and the value for r_b derived from Fig. 11 may be used with confidence to evaluate motor performance at 60V for $0 < I \lesssim 25$.

With the added resistors in the armature winding and the brush leads, the current was held below its normal rated value of 40 A for these tests. Heating losses in these components cause the efficiency in Fig. 12 to peak at about 80%. This figure is higher without these added resistors, and performance characteristics obtained on the machine prior to modification of the armature (Fig. 13) show a peak efficiency of 85%. In this case, the armature winding resistance was .042Ω, and the brush contact resistance of .152Ω represented 78% of the total resistance. This high proportion is indicative of a problem occurring at the brush contacts, and this will be shown to be the source of the dominant power loss in this machine.

4. Commutation Power Losses.

The objective is to compute the power loss associated with short-circuit currents during commutation, and to determine whether they appear in Fig. 11 as part of the constant term, P_ℓ, or the variable I^2R_a loss.

4.1 Short-Circuit Currents during Commutation.

Equations (1) and (2) are solved for the mesh current i_1 (Fig. 3), which will be zero at the onset of commutation for the short-circuited coil, and will only vary through the mutual inductance with i. This is due to the path chosen for i_1, and hides the fact that direct terminal current flows in both of these neighboring paths, through the brush

resistances r_{b1} and r_{b2}. Clearly, this was taken into account when deriving values for r_{b1} and r_{b2} from the constant speed test, and these resistances should now be used with the appropriate currents. This is achieved by setting the initial and final values of i, at the onset and end of commutation, equal to the normal path current.

As an example, a terminal current of 24.4A will divide into the 8 parallel paths, giving initial and final values for i of -3.05A and +3.05A. At the onset of commutation for the coil in Fig. 3, it has just emerged from the right-hand neighboring path, and the initial current of -3.05A accounts for the losses in the r_{b1} and r_{b2} contacts in <u>that</u> path. The power losses in the contacts in the left-hand path are equal to this, being accounted for by another coil entering commutation at the next brush. There are, in fact, eight coils in the machine in the same condition corresponding to the eight parallel paths.

The calculated variation of current in a coil undergoing commutation is shown in Fig. 14, for operation at 60V, 24.4A, and a speed of 2171 rev/min derived from Fig. 12. Because the armature coils have very low inductance values, commutation is achieved very rapidly. Mutual coupling will cause a spike to appear on the current of the neighboring coils, and conversely, spikes appear on Fig. 14 at the instants when neighboring coils are commutated, these spikes should accumulate and appear on the terminal current waveform, and Fig. 15 shows the measured current entering one positive brush. The variations in the spikes are due to non-uniformities in the armature winding and the magnets.

The measured variation of coil current is shown in Fig. 16, for the same operating conditions. These oscillograms confirm the predicted rapid reversal of current at the onset of commutation, but show it rising to a higher peak than calculated during the first half of the commutation period. One possible cause of such a discrepancy would be if the brushes could tilt, commutation would be advanced and the peak current would increase. However, solution of Eqs. (1) and (2) showed that this effect would not yield the desired peak current.

It is postulated that the brush contact is not simply resistive, but is also capacitive. In that case, the path for the short-circuit current, i, in Fig. 3 forms a series resonant circuit, which would require a capacitance of about 480 μF at a resonant frequency corresponding to 2171 rev/min. If such a capacitance existed in a conventional machine, the normally much higher coil inductance would reduce the resonant speed to a very much lower value, and an effect such as this would not be detected. It is not expected that such an effect will have a simple relationship with terminal current, but it should still be evident for motor operation on no load. Figure 17 shows the coil current at 60V, 3.2A (no load), and indicates that the high current peaks do still exist, but are variable and somewhat unpredictable; this is typical behavior of brush contact phenomena. To support the theory that capacitance exists, close examination of the coil current on load (Fig. 16 (b)) shows that ringing occurs after the reversal of current at commutation.

4.2 Power losses.

From the calculated variation of i in Fig. 14, the power loss in the

coil can be evaluated for the entire commutation period. A similar variation, without the added resistor R in the coil, will yield the power in the other seven coils being commutated. The effect of terminal current has been accounted for in the initial and final values that were set for i, and so these eight coils represent the total commutation power loss. Some calculated values are given in Table I, together with the power loss in the other fixed resistances in this machine.

The total calculated electrical power loss at 2400 rev/min is subtracted from the measured curve in Fig. 11. The mechanical power loss at this speed was measured by demagnetizing the stator of the experimental machine, and by driving it with another iron-less axial-field motor. There remains a further component of the total losses in Fig. 11, which is also associated with the commutation process. If this component is added to the proportion of the calculated electrical loss already attributed to commutation, then the commutation power loss is represented by:

$$P_{comm} = 145 + .152\ I^2\ (W). \qquad (14)$$

Comparing this to the total power losses given in Eq. (13), commutation accounts for 76% of the constant component, P_ℓ, 49% of the current dependent component in the experimental machine, which would be 78% of I^2R_a in the machine prior to modification of the armature.

That the commutation power loss is significantly independent of armature current, is supported by the oscillograms of short-circuit current, which show that the peaks at the onset of commutation on load (Fig. 16) are still present on no load (Fig 17).

Table I: Calculated I^2R power losses for 60V supply, using r_b measured at 2400 rev/min.

Terminal current, I (A)	Total commutation power loss (W)	I^2R loss in winding and all added resistors (W)	Total I^2R power loss in motor (W)
3.2	8.1	1.6	9.7
18.0	87.7	50.9	138.6
24.4	154.0	93.5	247.5

Armature reaction, not present in this machine, would cause this power loss to be more heavily dependent upon terminal current. Although the total power losses may be represented by Eq. (13), from which a steady value for r_b was deduced, this resistance does not have to account for the entire brush contact loss. That is, the brush contact does not have to be simply the constant r_b as seen through the terminals. The evidence is that the contact should be modeled also by a reactive term, chosen such that the circulating current matches the oscillograms (Figs 16, 17).

5. Conclusions.

Despite having a large proportion of its losses attributed to unwanted circulating currents in coils during commutation, this experimental disc-armature motor exhibits a peak efficiency of 85% at rated current, and maintains above 80% efficiency over a wide current range from about 15A to several times rated current (Fig. 13). This commutation power loss is evident even without load, and must be considered to be the major problem in obtaining optimum performance from this type of low inductance machine. The ironless armature gives benefits such as elimination of rotational iron losses and armature reaction, but these must be weighed against the effects of having significant field in the magnetic neutral regions, creating the e.m.f. that drives the short-circuit currents. Under current investigation is the inclusion of magnetic wedges between coil sides in the armature, to enhance and constrain the field under the poles, these wedges being made from a low loss iron powder composite.[7]

Since commutation power loss is the critical problem in this machine, analysis should be performed using an equivalent circuit as described here.

However, it is apparent from the oscillograms that Fig. 3 may not be complete, because the short-circuit currents and power losses were found to be predominantly independent of terminal current. Therefore, whatever impedance is used for the brush contact should be derived from measurements of the circulating current, rather than the terminal current. Further and more detailed studies using this technique to measure i will be required to determine that impedance.

The very low values for the inductances in this machine cause commutation to occur very rapidly, leaving a coil short-circuited for a much longer period than is necessary simply to reverse the current. The benefit of having higher inductances appears to be that they would eliminate any resonance that is causing i to rise to such high measured values. This paper has described the calculation of inductances in this permanent magnet machine, and so the effect upon performance of adding any magnetic material to the armature could be computed. In this case, the properties of the permanent magnets adjacent to the air-gap will be important, and for the anisotropic Alnico 5-7 described here, the recoil permeabilities in the preferred and transverse directions are quite different. Commutation occurs with the coil and pole axes coincident, the position of minimum coil self-inductance in this type of machine. Current research is aimed at broadening the investigation to other important types of permanent magnet material, in particular Alnico 8, to compare the effect of different field distributions upon the short-circuit currents and power losses.

6. Acknowledgements.

The research described in this paper was supported by the NASA-Lewis Research Center (grant #NSG-3243), as part of the U.S. Department of Energy's Electric and Hybrid Vehicle Program.

7. References.

1. CAMPBELL, P.: "Principles of a permanent magnet axial-field d.c. machine," Proc. I.E.E., 1974, 121, pp. 1480-1494.

2. CAMPBELL, P.: "Performance of a permanent magnet axial-field d.c. machine," I.E.E. Jour, Elec. Power Appls, 1979, 2, pp. 139-144.

3. SHOBERT, E.I.: "Commutation," A.I.E.E. Trans., 1962, 81, pp. 594-601.

4. HOLM, R.: "Electric Contacts Handbook," Springer, Berlin, 1958.

5. CAMPBELL, P., and AL-MURSHID, S.A.: "The effect of the magnetization distribution within anisotropic alnico magnets upon field calculation," I.E.E.E. Trans, 1980, MAG-16, 1032-1034.

6. CAMPBELL, P., CHARI, M.V.K., and D'ANGELO, J.: "Three-dimensional finite element solution of permanent magnet machines," I.E.E.E. Intermag Conf., Grenoble, 1981, paper 21-6.

7. CAMPBELL, P., and NAFISI, A.: "The effect of iron powders on the utilization of permanent magnet materials in advanced motors," I.E.E.E. Trans, 1980, MAG-16, 690-692.

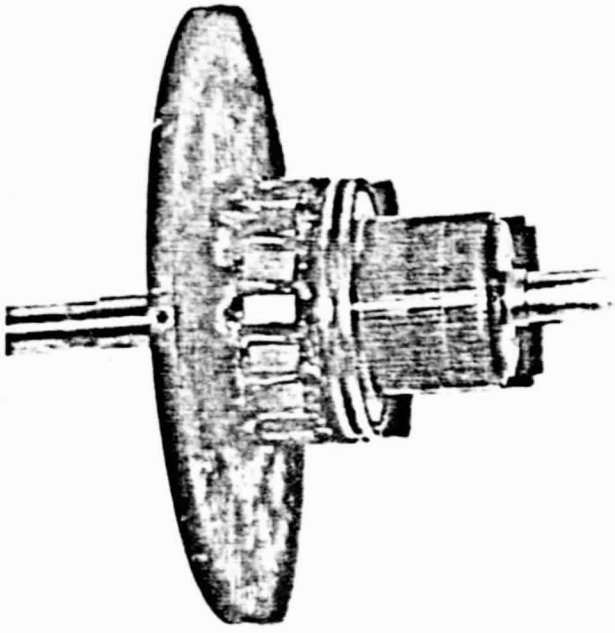

Fig. 1: Armature of the experimental machine, showing added resistors (two in parallel for 0.12Ω in every eight coil), one connected to silver slip rings.

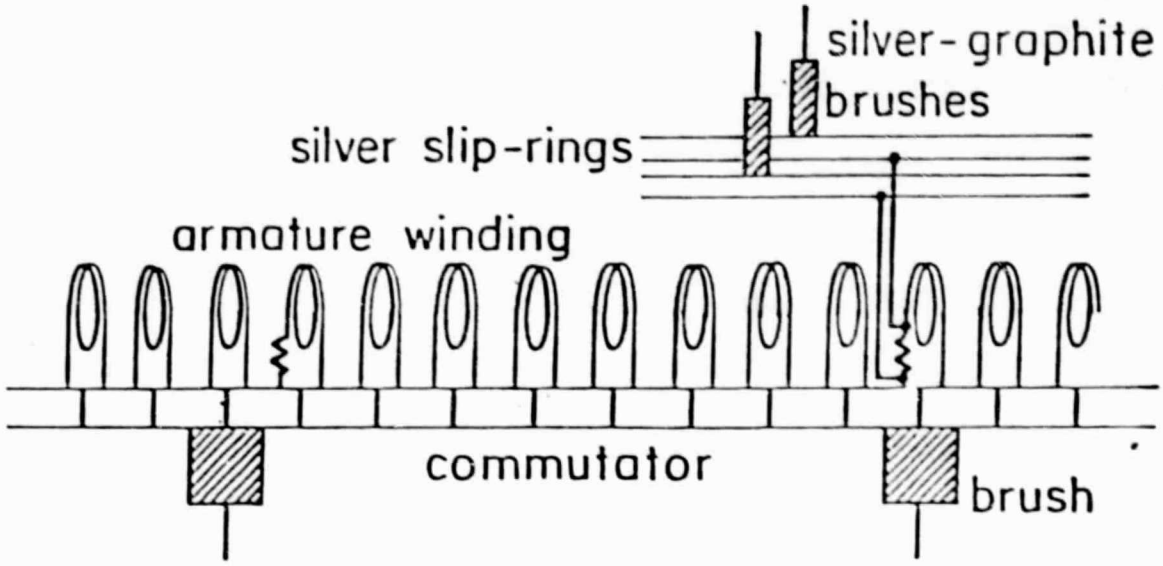

Fig. 2: Layout of part of the 72 coil armature winding, showing 9 coils/pole with a resistor added every eight coil, and brush arc = segment arc.

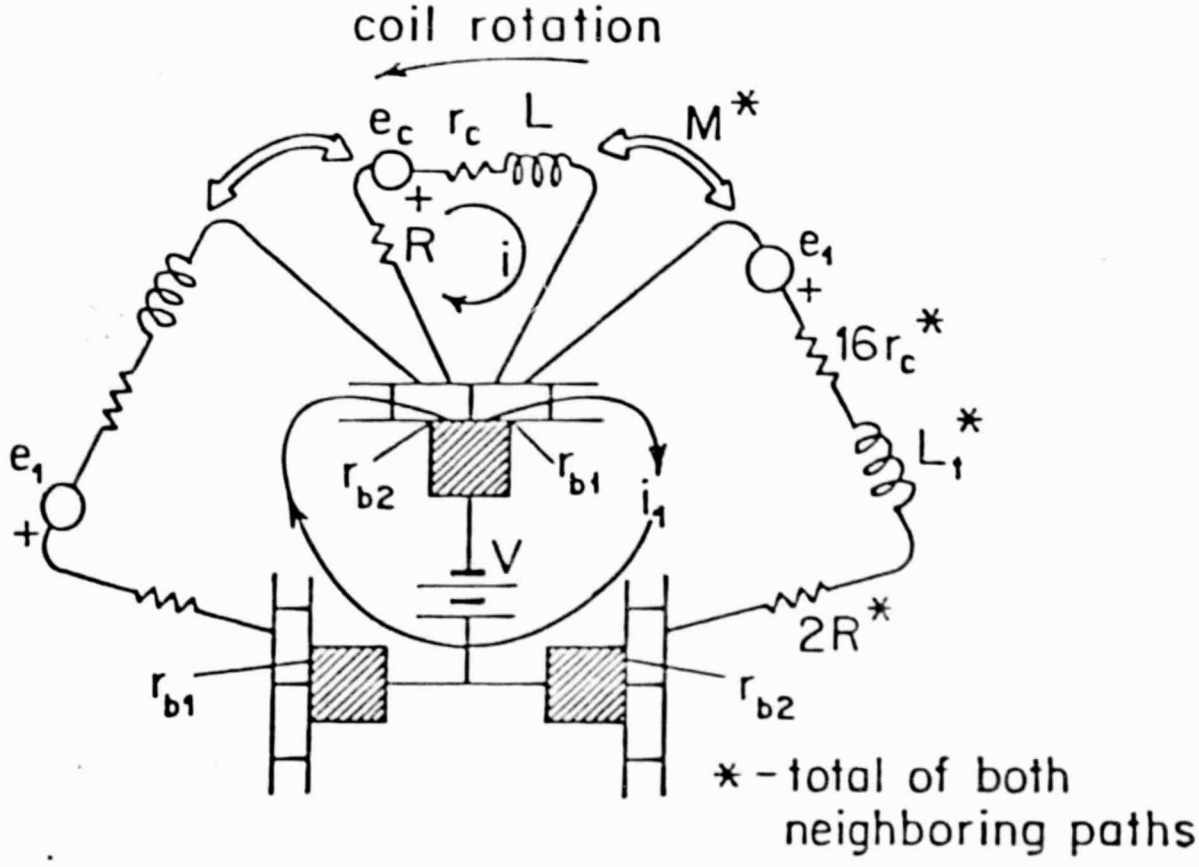

Fig. 3: Equivalent circuit for a coil undergoing commutation and its neighboring paths, showing mesh currents i, i_1.

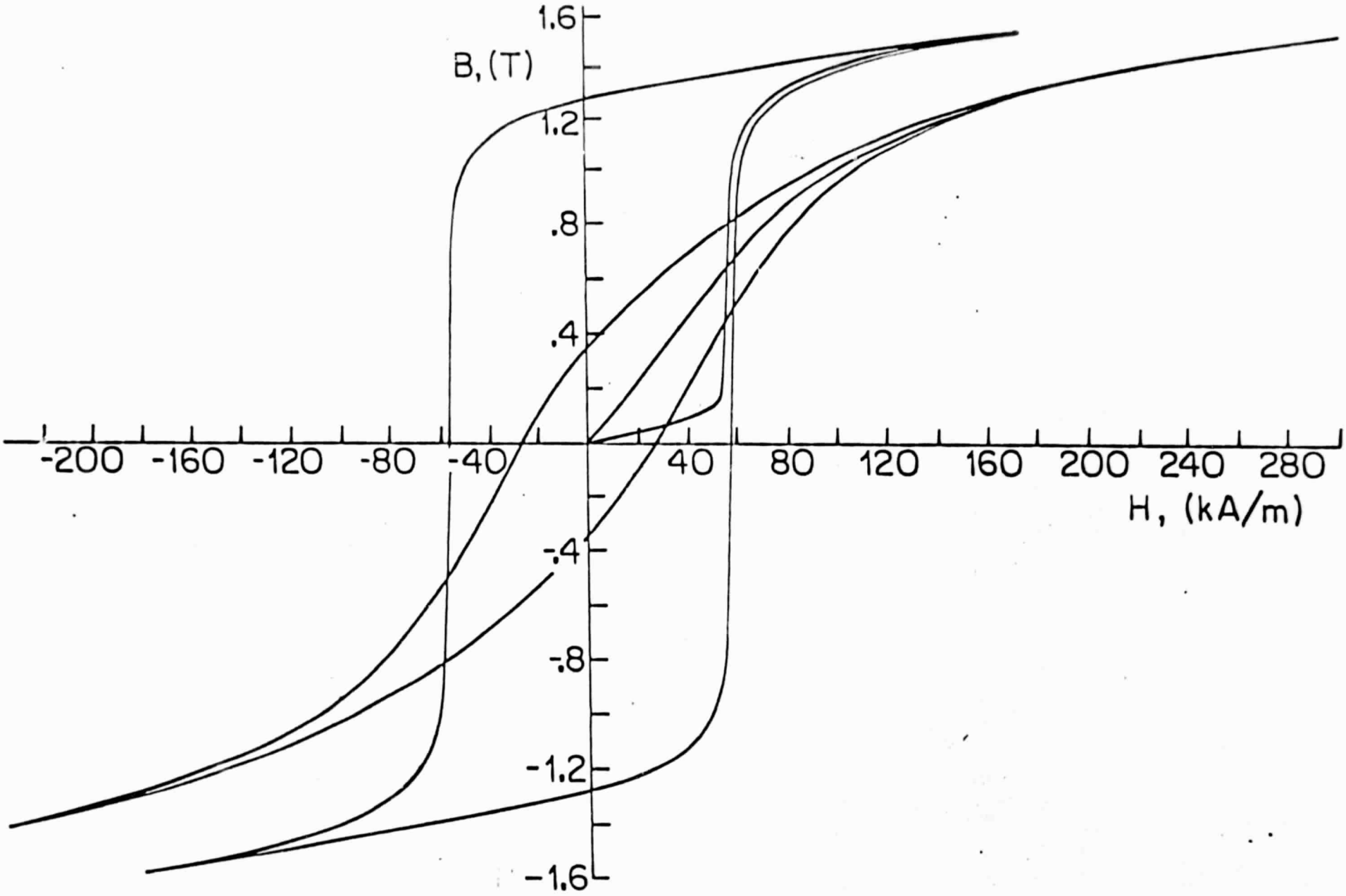

Fig. 4: Major magnetization loops measured for Alnico 5-7 in the preferred and transverse directions.

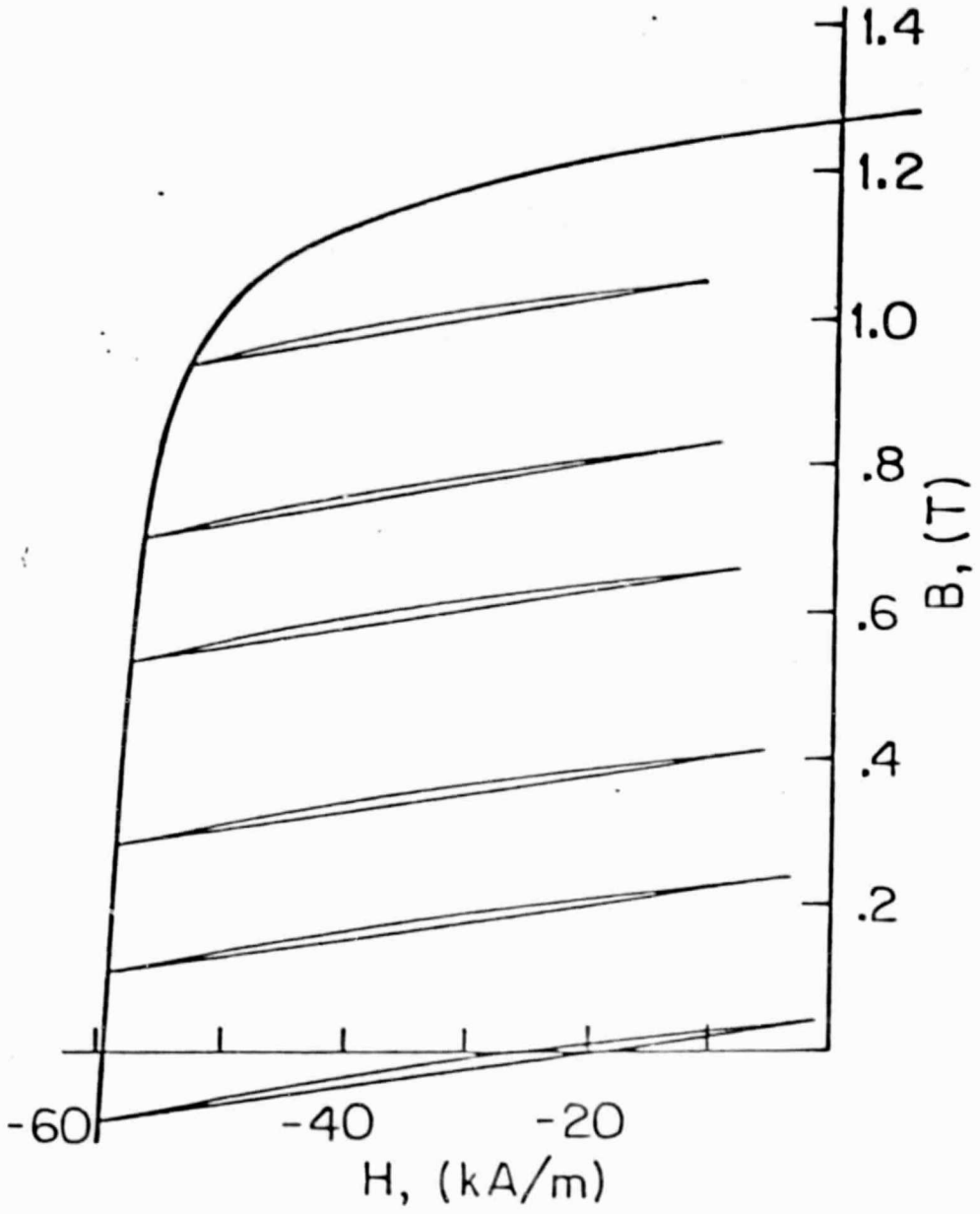

Fig. 5: Recoil loops in the second quadrant measured for Alnico 5-7 in the preferred direction.

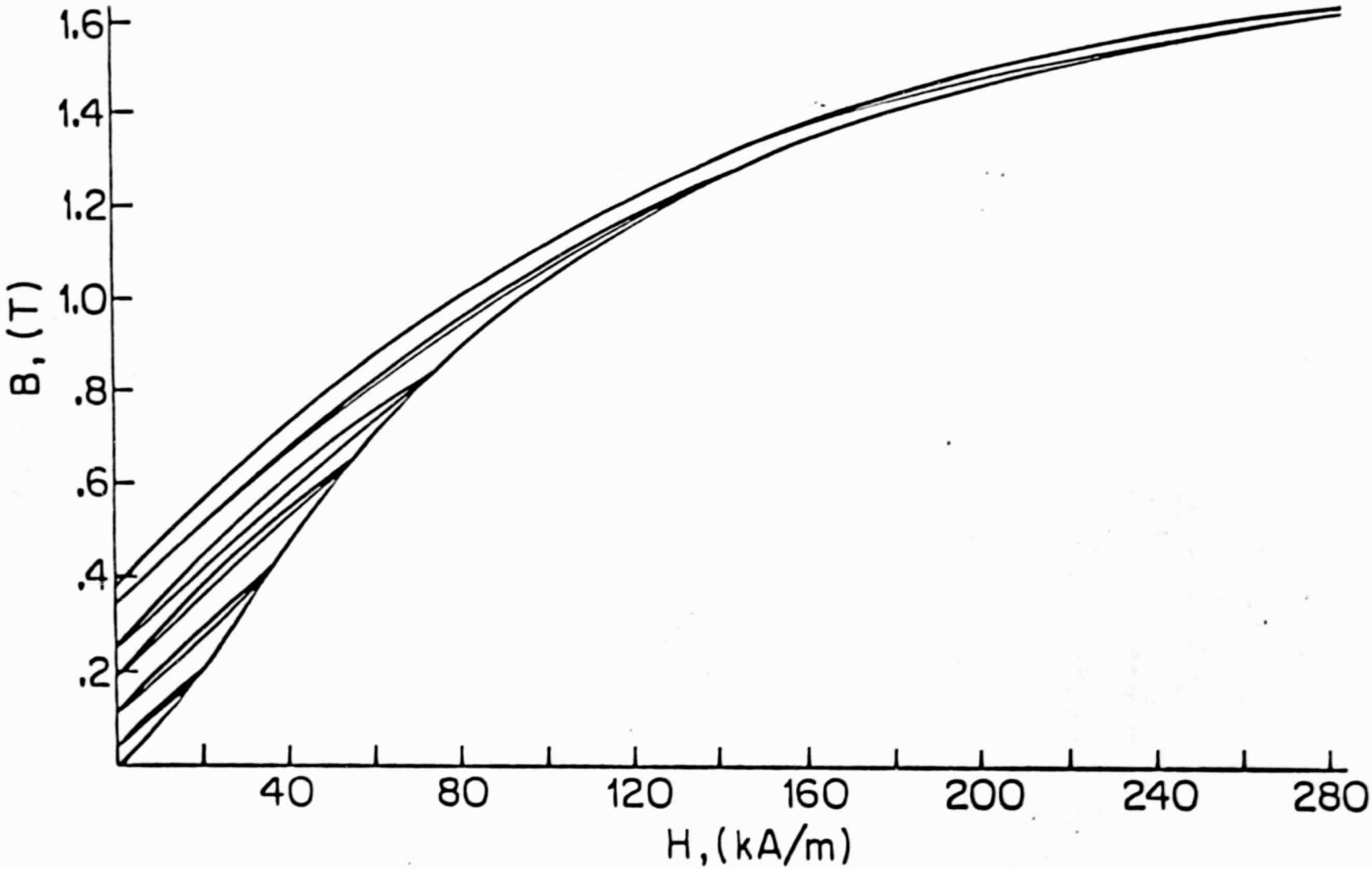

Fig. 6: Recoil loops in the first quadrant measured for Alnico 5-7 in the transverse direction.

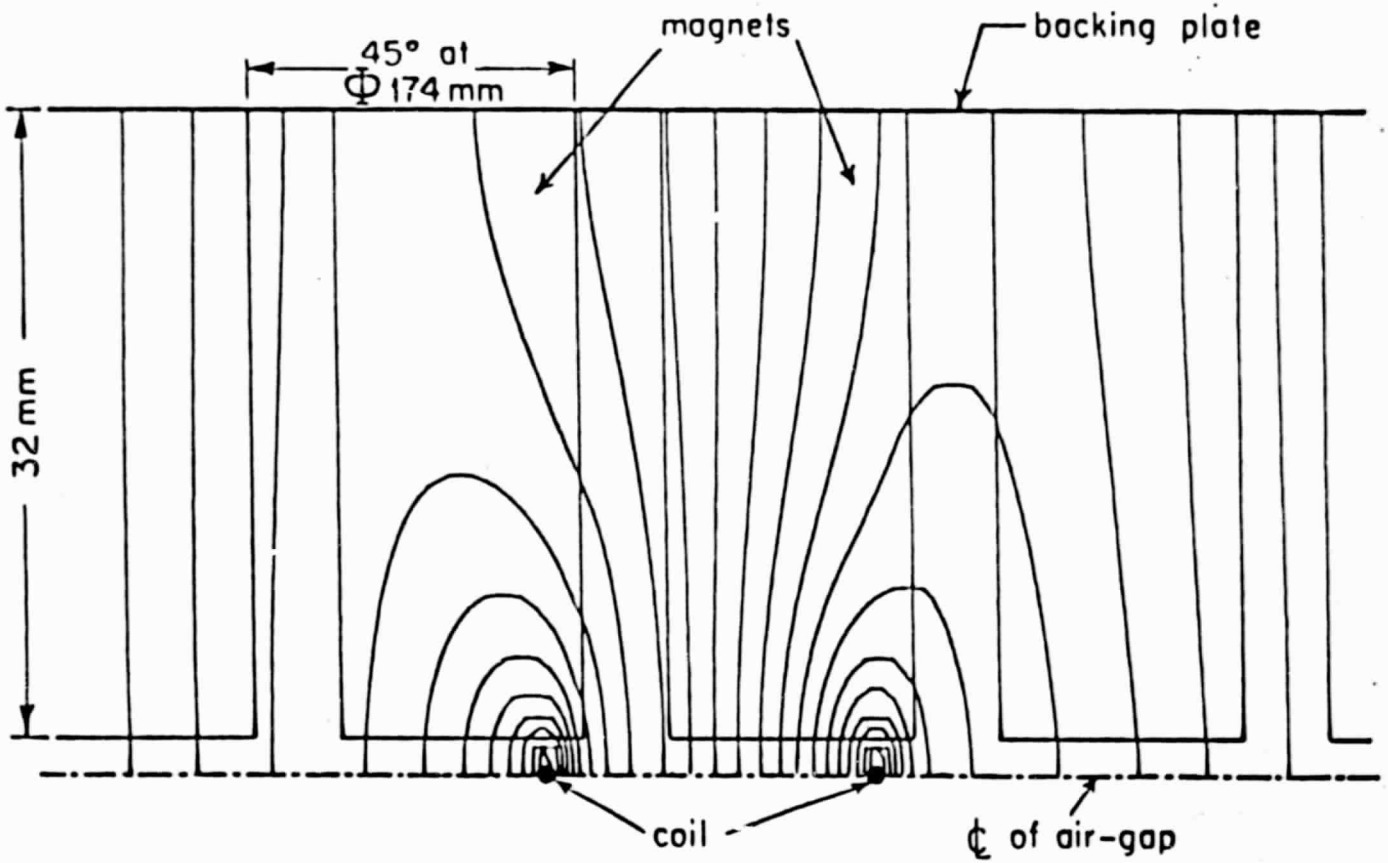

Fig. 7: Part of the field distribution calculated at the average active radius for rated current (5A) in a coil, whose axis is midway between a magnet center-line and magnetic neutral.

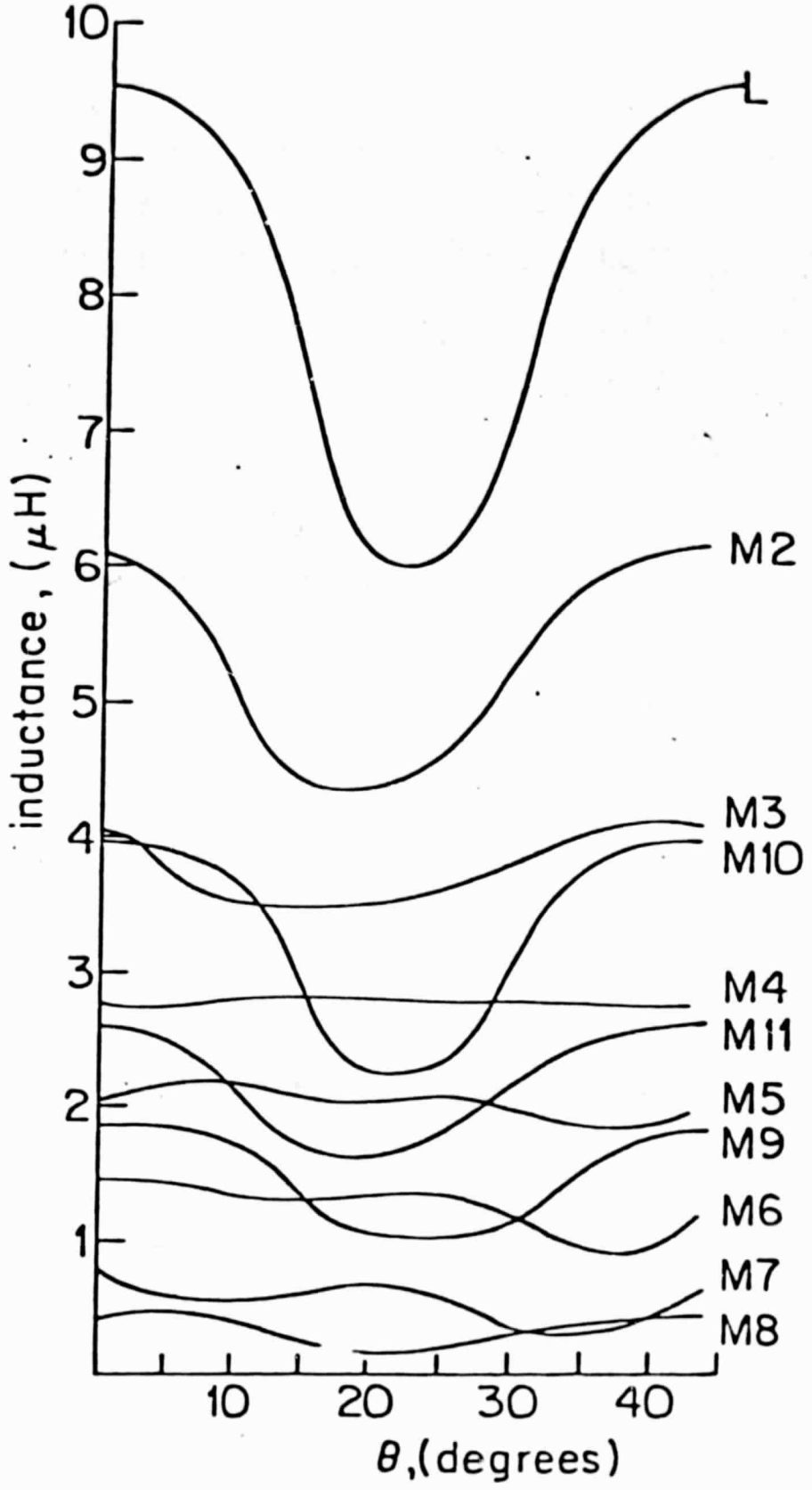

Fig. 8: Calculated variations of the self-and mutual inductances with the source coil axis θ^{o} from the magnetic neutral.

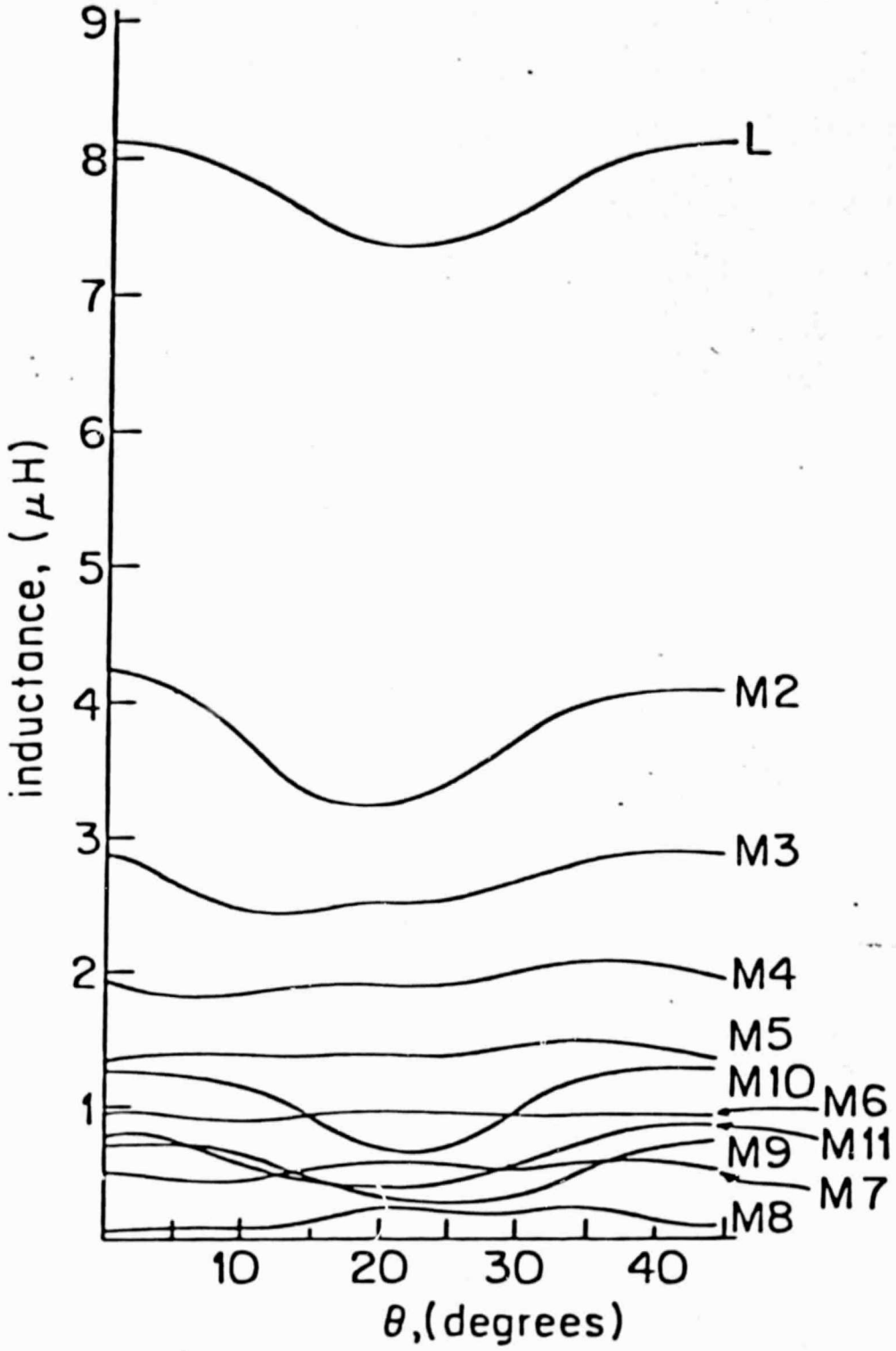

Fig. 9: Measured variations of the self-and mutual inductances with the source coil axis Θ^{0} from the magnetic neutral.

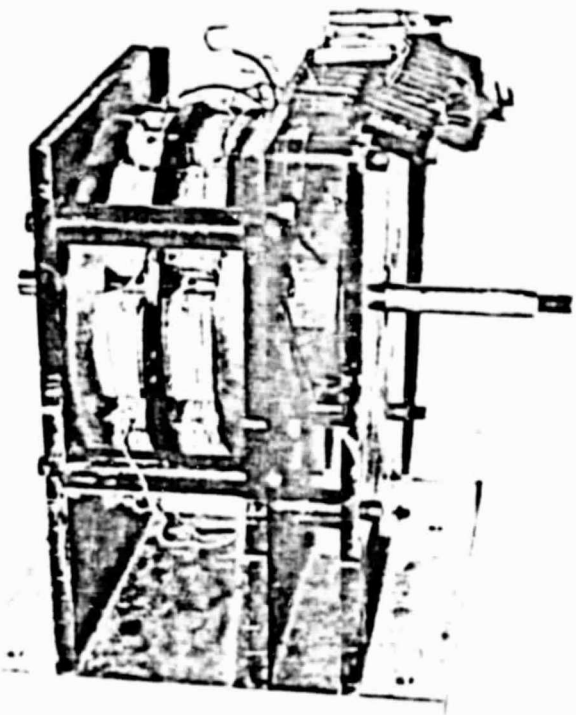

Fig. 10: The experimental disc-armature motor, with one set of Alnico 5 magnets either side of the armature, showing resistors connected in the brush leads.

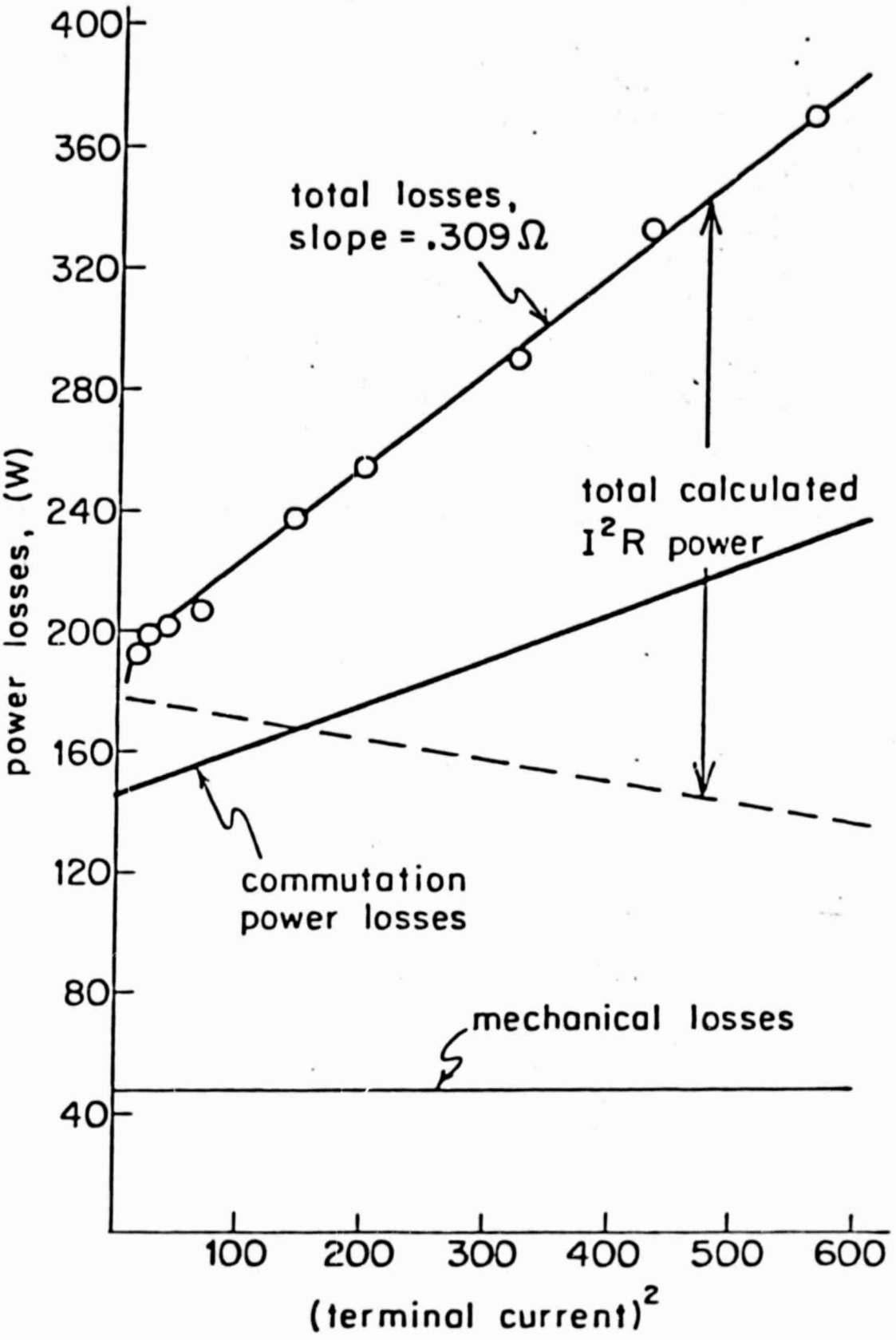

Fig. 11: Total power loss measured at constant speed = 2400 rev/min for the experimental machine, after modification with added resistors, showing components of the losses.

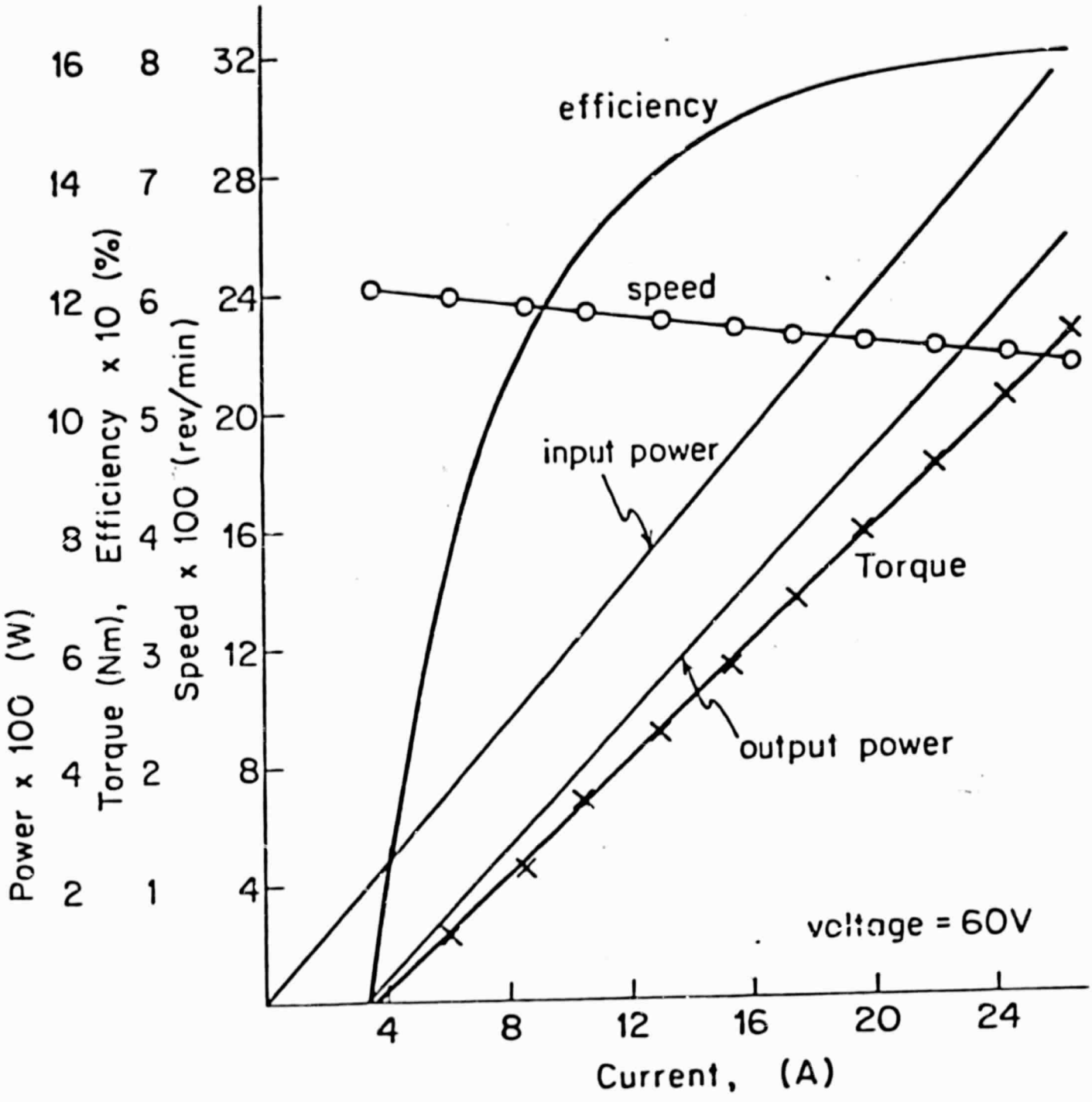

Fig. 12: Performance curves at 60V for the experimental machine, after modification with added resistors.

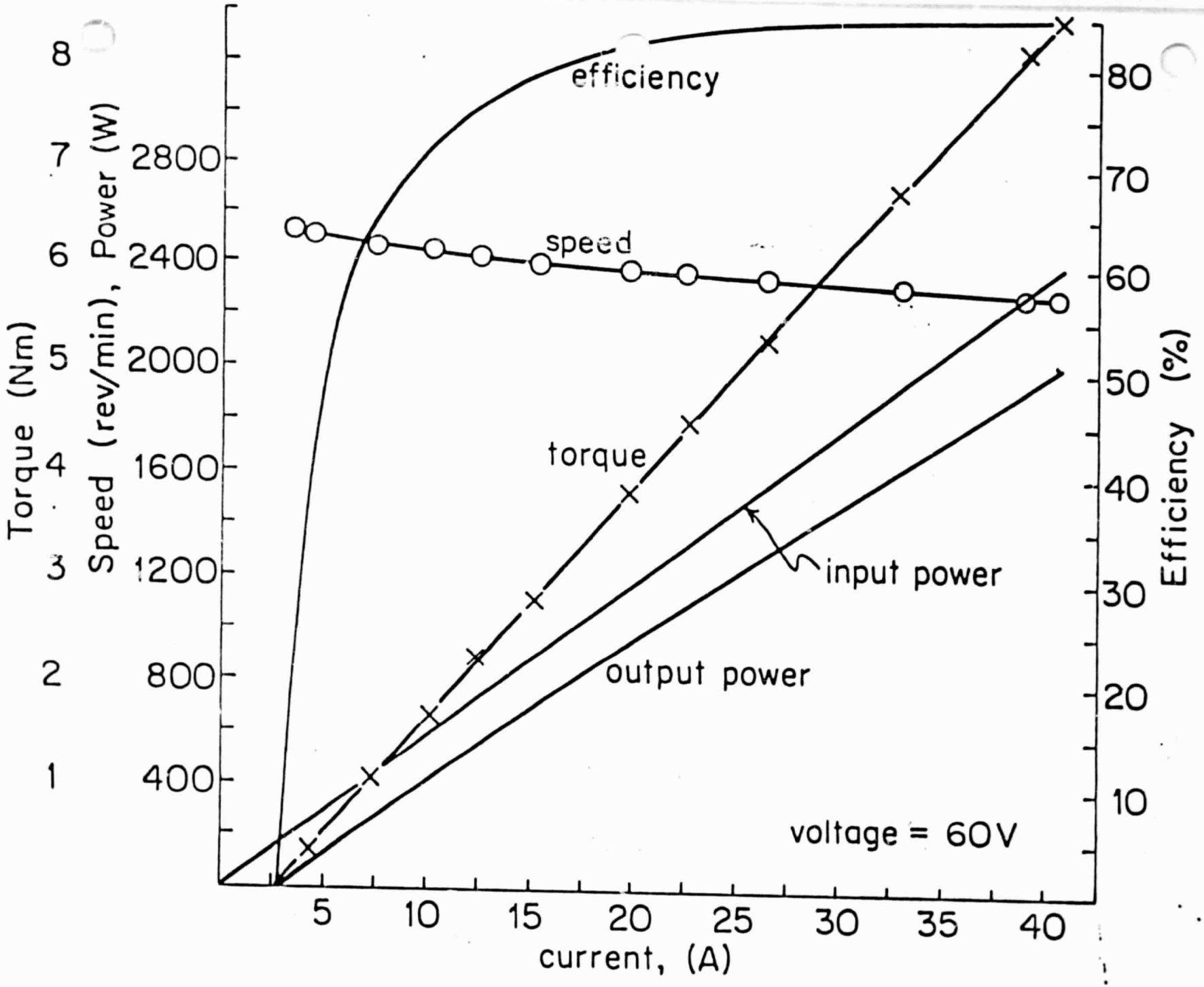

Fig. 13: Performance curves at 60V for the experimental machine with the original (unmodified) armature.

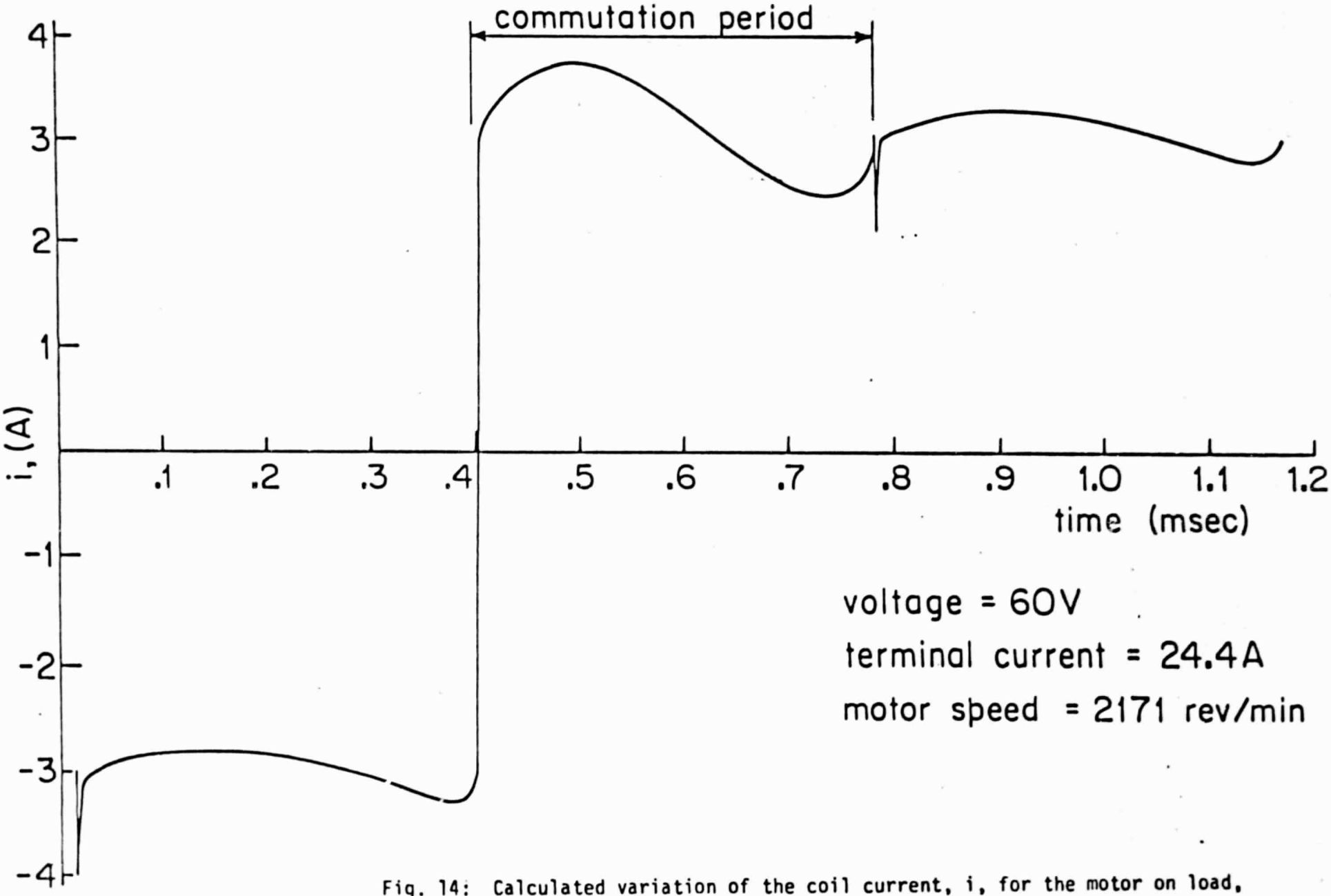

Fig. 14: Calculated variation of the coil current, i, for the motor on load, showing the commutation period.

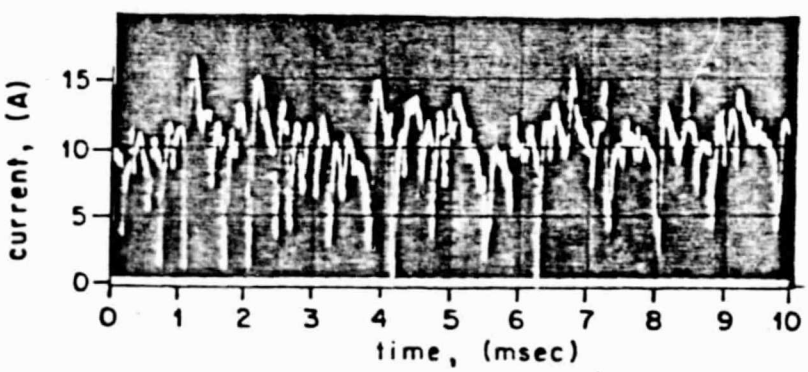

Fig. 15: Current entering one brush, for the machine operating at 60V, 24.4A, 2171 rev/min.

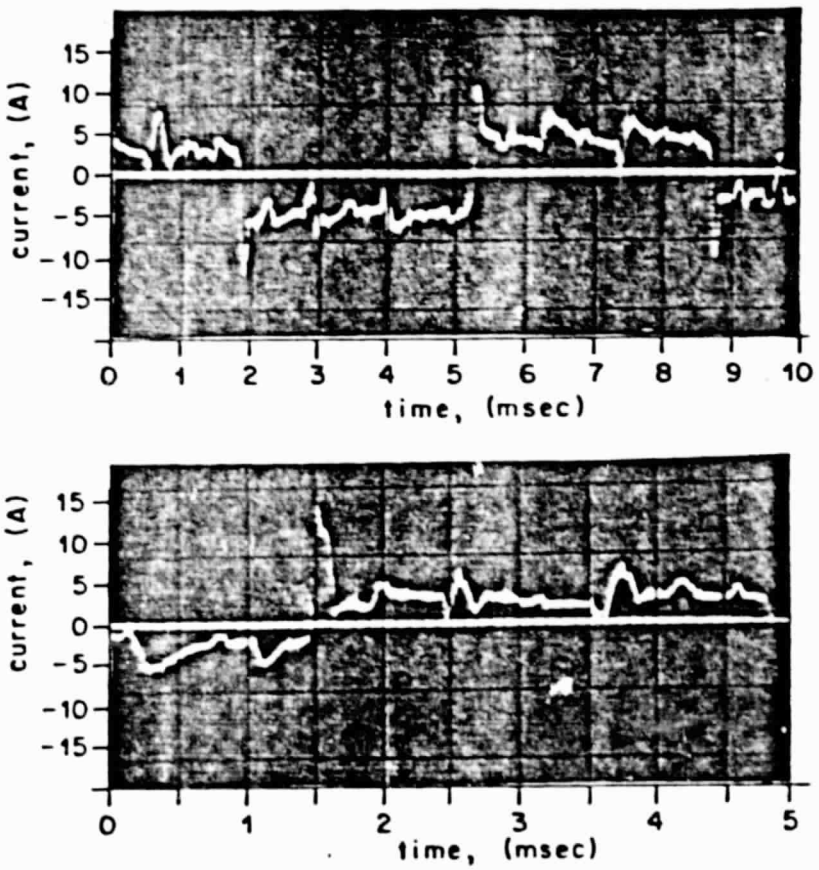

Fig. 16: Measured variation of the coil current, i, for the motor operating at 60V, 24.4A, 2171 rev/min.

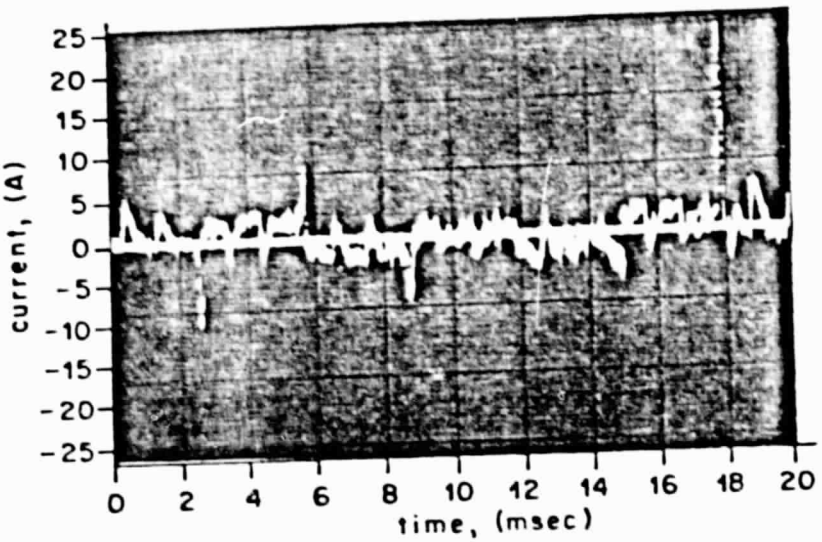

Fig. 17: Measured variation of the coil current, i, for the motor operating on no load at 60V, 3.2A, 2416 rev/min.